HHS Public Access

Author manuscript

Invest Radiol. Author manuscript; available in PMC 2016 September 01.

Published in final edited form as:

Invest Radiol. 2015 September ; 50(9): 657–670. doi:10.1097/RLI.0000000000000188.

Ultrasound in Radiology: from Anatomic, Functional, Molecular Imaging to Drug Delivery and Image-Guided Therapy

Alexander L. Klibanov, Ph.D.[1,2] and **John A. Hossack, Ph.D.**[2]

[1]Cardiovascular Division; Robert M. Berne Cardiovascular Research Center, University of Virginia School of Medicine, Charlottesville VA 22908

[2]Department of Biomedical Engineering, University of Virginia, Charlottesville VA 22908

Abstract

During the past decade, ultrasound has expanded medical imaging well beyond the "traditional" radiology setting - a combination of portability, low cost and ease of use makes ultrasound imaging an indispensable tool for radiologists as well as for other medical professionals who need to obtain imaging diagnosis or guide a therapeutic intervention quickly and efficiently. Ultrasound combines excellent ability for deep penetration into soft tissues with very good spatial resolution, with only a few exceptions (i.e. those involving overlying bone or gas). Real-time imaging (up to hundreds and thousands frames per second) enables guidance of therapeutic procedures and biopsies; characterization of the mechanical properties of the tissues greatly aids with the accuracy of the procedures. The ability of ultrasound to deposit energy locally brings about the potential for localized intervention encompassing: tissue ablation, enhancing penetration through the natural barriers to drug delivery in the body and triggering drug release from carrier micro- and nanoparticles. The use of microbubble contrast agents brings the ability to monitor and quantify tissue perfusion, and microbubble targeting with ligand-decorated microbubbles brings the ability to obtain molecular biomarker information, i.e., ultrasound molecular imaging. Overall, ultrasound has become the most widely used imaging modality in modern medicine; it will continue to grow and expand.

Introduction

Over the decade 2000–2011, the annual global per-procedure usage of X-Ray Computed Tomography (CT) and Magnetic Resonance Imaging (MRI) doubled [1]. Meanwhile, the number of ultrasound imaging procedures increased more than tenfold [1]. It is clear to practicing radiologists that this increase in ultrasound imaging usage has not occurred in the traditional medical imaging settings - radiology and cardiology departments in hospitals. In this review, we will examine recent developments and potential future directions in ultrasound imaging instrumentation that will explain the rapid changes in the practice of medical ultrasound imaging.

Correspondence address: A.L. Klibanov, UVA CVRC, PO Box 801394, Charlottesville VA 22908-1394., sasha@virginia.edu; sklib1@gmail.com, Phone + 1(434)243-9772 (lab); + 1(434)466-3821 (cell); + 1(434)9823183 (fax).

Similar to the other imaging modalities, ultrasound is approaching limits imposed by the underlying physics (e.g. wavelength) and regulatory tolerance for patient exposure to any form of energy transmitted into the body. Therefore, it becomes interesting to speculate how the different modalities may evolve in the coming years in the face of fundamental physics-origin limitations. As in other imaging modalities, application of contrast agents may assist in overcoming some of the limitations, and brings ultrasound imaging to the areas where its application was not feasible earlier, such as molecular imaging, therapy and drug delivery. In a short manuscript format it is not possible to provide an exhaustive review of literature; we provide examples of the specific trends of highest interest.

Fragmentation of the Practice of Ultrasound Imaging

Until the early 2000s, ultrasound imaging was dominated by cart-based systems priced in the ~$100–200K range. Physicians, or specialized imaging technicians, in hospital radiology and cardiology departments operated these instruments. More recently, ultrasound imaging has proliferated in the form of hand-held and laptop-size instruments that are finding use in a range of settings beyond conventional large hospital imaging-focused departments. By extension, the reduced size, reduced cost and perceived reduced training requirement of these smaller devices make them feasible options for overseas and underserved communities, as well as ambulance and house call scenarios. This change has been enabled by the Moore's Law [2] related improvement in the performance of electronics. Specialized, single purpose, signal processing hardware has been replaced by systems in which software controls a range of functions implemented on powerful, versatile, digital processors with very high data bandwidths [3, 4]. Today's hand carried instruments can essentially achieve functionality and imaging performance similar to the earlier cart-based instruments [5]. Small-scale instruments are finding uses that include guiding vascular access [6], emergency room assessment for conditions such as chest pain [7], detecting blood pooling or foreign object identification / removal [8]. Significantly, these instruments are primarily operated by healthcare workers for whom imaging is not their primary clinical specialty. Medical ultrasound has been taken to the International Space Station [9] and to the battlefield [10]. Remote real-time image viewing (i.e. "telemedicine") has been demonstrated in both scenarios [9, 10].

Figure 1 illustrates two recently commercialized handheld ultrasound scanners. It is clear that we are approaching a scenario in which size of the device is not limited by electronics but by the need for a transducer of a specific aperture according to the clinical necessity and the requirement for a usefully dimensioned image display. Currently, battery dimension and charge duration are also significant considerations but progress in battery technology and processor efficiency provide optimism for continued improvement towards a widespread use of handheld and laptop-based ultrasound.

In essence, the Moore's Law contribution to the field is greatest in areas where massive computational processing requirements are most relevant. Until recently, many of signal / image processing algorithms that existed only in research laboratories could not be translated to widespread clinical usage. Now, however, progressively more complex signal and image processing tasks come within the realm of practicality and viable cost.

Each imaging modality is capable of anatomic, functional and molecular imaging – with varying degrees of performance and limitation. Anatomic imaging remains the dominant application even as the increasing values of functional and molecular imaging become more evident. Unfortunately, ultrasound imaging does not reliably perform well at anatomic imaging. Ultrasound relies on weak reflections and low rates of beam refraction. Generally, in soft tissue, the weak reflection requirement is met. The weak reflection requirement is not met when there is an interface involving materials possessing significantly different acoustic impedances. In ultrasound, bones and air volumes (in lungs, esophagus, and the gastrointestinal tract) present challenges and give rise to limited "acoustic windows" in some applications. For example, cardiac imaging relies on a relatively small number of acoustic windows between or below the ribs. The weak reflection requirement is not met in some other scenarios giving rise to either, or both, acoustic shadowing and acoustic reverberation. In the former, ultrasound does not reach underlying tissue regions and no echo signal is received resulting in a black region. A typical example involves the inability to "see" below an overlying rib. Reverberation typically occurs between overlying layers of muscle and fat and causes multi-path reflection [11]. This is projected as a phantom, static, echo haze-like image appearing at a greater depth than the actual source of the initial reflection. In radiology applications, the "haze" obscures the tissue of interest to varying degrees contributing to reduced image contrast and less reliable diagnosis.

This phenomenon occurs in cardiac imaging and may cause a static haze over the superficial moving cardiac muscle or appears, for example, as a static object within a heart chamber. Another important class of ultrasound artifact frequently encountered relates to "phase aberration". Ultrasound beam formation relies on assumed tissue velocity. Since fat possesses a significantly lower sound speed (1478m/s) than muscle tissue (1547 m/s) [12], a layer of non-uniformly thick superficial fat, or distributed fat, can give rise to refractive errors in the beam focusing process. This results in a degraded beam resolution that has impact on both image spatial ("detail") resolution and image contrast quality. These artifact mechanisms give rise to a variety of opportunities in research and point towards areas of probable progress in the coming decade.

Phase aberration correction

Phase aberration has been extensively studied since the late 1980s [13]. Flax and O'Donnell's work represented a major early contribution towards a practical solution in that it was the first to not require a "beacon" or ideal point source. During the 1990s, efforts were made to implement phase aberration correction on clinical scanners but cost and technical complexity impeded progress. Additionally, it was realized that ideal phase aberration correction requires aberration delay correction in both elevational and azimuthal dimensions on an array surface [14, 15]. Building from the concept of receive direction phase distortion, Liu and Waag proposed a "back propagation" approach in which compensatory delay corrections are made on the transmit direction [16]. A closely related technique involves the use of "time reversal" which also uses received phase errors to guide subsequent transmitted waves [17]. This technique works optimally with a well defined point source or point scatterer. More recently, Pernot [18] proposed the generation of cavitation bubbles to provide a nearly ideal source for the time reversal approach. Considerable work over many

years has resulted in progressively more sophisticated algorithms with improved performance versus the earlier element signal cross correlation approaches. These include development of a new generalized coherence factor (GCF) [19] in which the lower frequencies correspond to the phase aligned components of received echo data, and the higher frequencies correspond to the poorly phase aligned echo signals. Additionally, new applications are being proposed that include, for example, phase aberration correction to improve the performance of therapeutic transcranial focused ultrasound [20–23].

"Tissue Harmonic Imaging" (THI)

Nonlinear ultrasonic propagation effects have been studied for several decades. During propagation at high pressure levels, local sound speed changes between compressional and rarefactional phases giving rise to distortion of the wavefront. This progressive increase in signal distortion gives rise to the presence of harmonics of the transmitted signal and these harmonics can be isolated for imaging purposes. Christopher, in 1997 [24], focused attention on the potential impact of imaging using the tissue harmonic signal and, in particular, it was noted that the nonlinear tissue signal would have reduced sidelobes and improved performance when propagating through typical abdominal wall sections. Within a few months following this paper, all major ultrasound imaging equipment vendors offered some variant on tissue harmonic imaging. In current imaging usage, THI, rather than conventional fundamental mode imaging, is frequently the default operating mode [25]. Initially, it had been assumed that the low signal level of the nonlinear signal would be objectionable but practical experience indicates that the level of performance achieved in practical settings vastly outweighs a relatively modest impact on maximum imaging depth. One minor drawback of tissue harmonic imaging is that it has motivated widespread use of higher peak power intensity in order to generate the greatest nonlinear signal and to minimize the impact of reduced SNR. Tissue harmonic imaging has proven to be one of the major contributions towards improved clinical B-Mode ultrasound quality [26, 27]. Significantly, tissue harmonic imaging made the greatest clinical impact in imaging through the abdominal wall of patients with thicker abdominal walls – i.e. it has made the most impact in the population most likely to benefit from diagnostic ultrasound. It is only in recent years that comprehensive simulations, enabled by high power computation, have elucidated the underlying roles of phase aberration and nonlinear signal generation in the remarkable improvements in image quality observed in clinical THI imaging [28].

Model-based segmentation and imaging

Frequently, in radiology it is desirable to assess the shape or volume of a particular tissue region. In the case of objects with well-constrained shapes it becomes feasible to eliminate imaging deficiencies (overlying noise, speckle effects, etc.) by fitting a model to the acquired data and presenting to the user a model closely fitted to the acquired image data. For example, a tumor mass or the left ventricle of the heart is known to possess a convex shape that can be fitted and presented to the user as a perfectly "clean" representation of the ventricle – with a seemingly realistic smooth surface and no overlying clutter. Once the model is determined, clinically important linear, area and volume dimensions may be reliably generated. The primary limitation of any model-based fitting approach is that if the

model is poorly selected then the method will fail to obtain an accurate fit to the actual available image data. In cancer radiology, there is interest in following the serial evolution of a tumor to assess growth or regression. The most reliable measure of tumor size is a determination of volume (3D) rather than a linear dimension (1D) or maximal cross-sectional area (2D). These two latter measurements are susceptible to error, due to incorrect slice plane selection and both implicitly rely on simplistic geometric assumptions relating linear dimension, or area, to volume. Unfortunately, tumors and other masses can take a number of shapes making model fitting challenging. One of the most versatile fitting models in image processing involves "snakes" or "active contours" [29]. Although originally developed as a 2D model, the snake is readily extensible to 3D [30]. The snake formulation involves the use of "internal energy" and "external energy" [29]. "Internal energy", which can be user refined, forces the fitted closed line (or volume) shape to adopt a controlled degree of smoothness. (Technically, this involves a constraint on the second derivative along the resulting snakes contour.) In the case of a noisy ultrasound image, this parameter is particularly important. "External energy" is the parameter that forces the fitted line to best conform to the underlying image data. This is most frequently derived from the image gradient (i.e. image feature edges). Since the purpose is to find the underlying feature gradient, uncontaminated by ultrasound image speckle, snake processing on ultrasound data frequency involves a speckle reducing pre-processing step [31, 32]. There are a number of frequently encountered speckle reducing algorithms [33–38]. Among these algorithms, Yu's Speckle Reducing Anisotropic Diffusion (SRAD) is the most commonly encountered and has been extended to 3D [39]. Several examples of the use of snakes in ultrasound feature segmentation exist for both 2D [40] and 3D [41, 42].

Artifact reduction

One of ultrasound's primary weaknesses as an anatomic imaging modality, in comparison with MRI and CT, is its susceptibility to artifacts. This motivates a range of efforts to solve ultrasound's artifact problems. Fortunately, evolving processing speed enables the clinical realization of progressively more complex algorithms. Except in the case of tissue harmonic imaging, in which the nonlinear second harmonic of the transmitted fundamental is isolated (i.e. filtered) for image formation, the challenge in ultrasound image data processing is that desired signals and artifacts (e.g. reverberations) cannot be isolated by simple frequency domain filtering.

Frequently, the contrast qualities of an image can be improved by spatial compounding in which a common tissue region is viewed from independently oriented transmit beam angles [43]. Spatial compounding has been shown to reduce speckle, clutter and improve image qualities and the ability to differentiate tissues [43]. In particular, it has proven successful in breast ultrasound: increased conspicuity of lesions, improved margin delineation and clearer cystic imaging have been reported [44]. A limitation, however, of transmit beam spatial compounding is that the aperture must be divided to yield independent apertures and this results in reduced resolution on a per aperture basis.

In the case of moving tissue one can, in principle, differentiate the desired moving signal from an overlying static haze artifact [45–47]. While most of these algorithms are

computationally intensive, they have the potential for widespread incorporation into the future generation of clinical scanners. This class of artifact reduction has more utility in cardiology than in radiology.

Quantification – tissue tracking

Within the past decade regional tissue tracking ("speckle tracking") has rapidly evolved from a research topic to a commonly implemented clinical ultrasound feature. Although most applications of speckle tracking are in cardiology [48–50], there are a number of radiology applications. Golemati et al [51] discussed the utility of speckle tracking for assessing elastic properties of the arterial wall and plaque in carotid arteries.

Advances in Doppler

Traditional Color Doppler processing is limited to detecting the 1D component of motion aligned with the ultrasound beam axis. Kasai's [52] 1D autocorrelation-based method formed the basis of the vast majority of early clinical scanner implementations for Color Doppler. Kasai's approach is computationally very efficient but involves a narrow signal bandwidth assumption. Kasai's approach was largely supplanted by Loupas' [53] 2D method which estimates the Doppler value using explicit estimates of both mean Doppler frequency and mean RF frequency at each range segment. It is also possible to estimate velocities using time domain cross-correlation [54] but this method is less frequently encountered in clinical implementations. However, all these early methods extract only the Doppler component aligned with the ultrasound beam axis. Given that vessels are frequently parallel to the skin surface (e.g. carotid artery), this represents a major limitation. In principle, this problem can be addressed using speckle tracking [55] but this typically requires high signal to noise ratio and, thus, is limited to shallow vessels like the carotid artery. Speckle tracking is also a relatively computationally intensive process. Another solution for enabling Doppler detection of transverse motion is to introduce oscillation into the transverse direction [56–58]. Using this approach, true "vector Doppler" (i.e. 2D Doppler) is achievable. Synthetic aperture-based approaches have also been proposed that transmit across all directions simultaneously and consequently can form images across the entire field of view at once [59]. By stepping the aperture source element across the array aperture, and combining the results from multiple transmit events, a high resolution wide-field Doppler image is acquired. More recently, there has been growth in the area of plane wave Doppler processing [60, 61]. Multiple acquisitions are obtained from multiple angles and these are combined. This approach provides for very high frame rates (>1000 fps vs. 10's fps in conventional Color Doppler) across wide fields of view (see Figure 2). Significantly, Bercoff notes that real-time implementation of this Doppler processing places very high demands on processor speed and data bandwidth [61]. Bercoff's work was implemented on the Aixplorer ultrasound system (SuperSonic Imagine, France). This is the first clinical system with the required processing capability for this new Doppler method and suggests where the "high end" of clinical ultrasound is evolving. Since kHz Color Doppler has only recently become available, we are only now learning about its value in diagnoses. It is also noteworthy that these frame rates place them well beyond the foreseeable capabilities

of competing imaging modalities even as frame improvements in competing modalities are enabled by significant technical advances.

Catheter-based ultrasound

Intravascular Ultrasound (IVUS) has been available clinically for more than two decades. Although the majority of IVUS applications are in cardiology, there are a number of uses within interventional radiology. IVUS technology generally divides into those based on mechanically scanned single transducer element and those comprising a solid-state circumferential array [62]. IVUS provides cross-sectional vessel anatomic structural information that is not obtained using only X-Ray angiography – which gathers information from a projection across the vessel lumen. IVUS also provides greater imaging depth than Optical Coherence Tomography (OCT); the latter is limited to ∼1 mm [63, 64]. IVUS can provide a range of functional information about the vessel wall health and function [63], yet OCT is frequently presented as a technology that may potentially supplant IVUS based on its superior spatial resolution. Recently, there has been significant progress in the area of pairing IVUS and photoacoustic imaging [65–68]. IVUS can provide excellent anatomic information and some functional information. Photoacoustic imaging provides superior information on vessel wall composition [66, 67] and can perform molecular imaging using appropriately targeted light absorbing nanoparticles [69] (see below).

Elastography

Early versions of elastography primarily relied upon an external application of force during which tissue motion was tracked in using phase sensitive approaches applied to the beamformed radio frequency (RF) line data [70, 71]. Over the years, many improvements have been proposed to the underlying algorithms to improve precision and accuracy [72–74] [75–77]. The method has found application in a range of settings that include: breast [78, 79], prostate [80] and thyroid [81]. The approach has been scaled down and performed using IVUS to assess vessel wall elasticity [82–84]. A major contribution in the field of elasticity involved the realization that acoustic radiation force could be used to project the force from within the body at a precise location instead of relying on an external force that rapidly decays with depth and is susceptible to artifacts due to intervening inhomogeneities [85–87]. This version of elasticity imaging is now in clinical usage [88]. More recently, considerable interest has arisen in shear wave elasticity imaging. Since a shear wave propagates slowly in tissue, the wavelength is low, which improves spatial resolution. Among the various implementations, supersonic shear imaging [89] appears to be the most promising and has yielded very encouraging early results. In this approach, a supersonic wavefront is created by rapid sequencing of pulses through depth, taking advantage of the fact that the shear wave velocity is just a few m/s. The method also relies on an ultrasfast scanner capable of full field imaging in response to a single transmit burst – i.e. similar to the Aixplorer ultrasound system previously mentioned. Promising results involving characterizing breast lesions have been reported using this approach [90]. It would appear that full frame, very high frame rate, systems like the Aixplorer most closely suggest the direction in which the “high end” ultrasound imaging field is going. It is also probable that a number of signal

processing techniques, yet to be invented, will be enabled by this versatile high performance architecture.

Photoacoustic imaging

Photoacoustic (or optoacoustic) imaging involves the use of short duration laser pulses to induce transient thermal expansions giving rise to emitted ultrasound pulses emanating from the point of light absorption. The received ultrasound pulses are processed in a manner analogous to conventional ultrasound receive signal processing. The receive path may involve either a mechanically scanned single element ultrasound transducer or a phased ultrasound array. Photoacoustic imaging has experienced an extraordinarily rapid rate of technical development in the past decade. Consequently, it should be viewed as a completely new imaging modality as opposed to a subset of ultrasound imaging. Photoacoustic imaging is discussed only briefly in this review. The reader is referred to the review article by Xu and Wang [91] for a more extensive discussion.

Anatomic ultrasound image contrast is a function of tissue mechanical properties, tissue interfaces and backscatter density. Image contrast in photoacoustic imaging is determined by local light absorption conditions and this will typically also vary with optical wavelength. Thus, it is feasible to image and differentiate between oxygenated and deoxygenated blood [91], differentiate lipid-dominant versus water-dominant tissue signals and detect other light-absorbing chomophores (endogenous and exogenous). Traditional optical imaging is sensitive to these parameters but possesses extremely limited penetration due to light scattering at any significant depth. Photoacoustic imaging is projected to contribute across a wide range of clinical areas that include: endoscopic imaging, mapping of metabolic rate of oxygen, melanoma, breast cancer, brain pathologies, and mapping of sentinel lymph nodes [92]. Photoacoustic tomography, using reconstruction principles similar to those used in Computed Tomography, has extended the technical frontier in terms of very high resolution photoacoustic imaging [93–95]. Using these approaches, small animal whole body photoacoustic imaging systems have become developed [96] and are available commercially [97].

Photoacoustic imaging divides broadly into two modes of operation. In acoustic resolution photoacoustics, it is not necessary for the input light to be focused to a single point. Because of rapid light scattering in tissue, in any event the light signal becomes defocused beyond approximately 1 mm of depth. In this scenario, photoacoustic imaging resolution is determined by the focusing performance of the receive ultrasound beamformation process. It is a common misperception to believe that light cannot penetrate deep into tissue. By choosing the correct light wavelength (i.e. using Near Infra-Red (NIR: ∼700 to ∼900 nm) [91], several cm of imaging depth is achievable. Additionally, photoacoustics has extensive applications in catheter-based applications where it can be paired with conventional IVUS [65, 66, 98]. Photoacoustics can also be paired with

Optical Coherence Tomography (OCT) [99].

Figure 3, from Hu et al, [100] illustrates a range of resolutions and sources of contrast that include optical resolution photoacoustic microscopy of sO2 in a mouse ear, acoustic

resolution photoacoustic microscopy of hemoglobin concentration in a human palm, photoacoustic CT of Methylene Blue concentration in a rat sentinel lymph node, photoacoustic CT of cerebral hemodynamic changes in response to whisker stimulation in a rat and Photoacoustic endoscopy of a rabbit esophagus and adjacent tissue.

Contrast agents in ultrasound imaging

Contrast materials are applied in all imaging modalities, and ultrasound is not an exception. Early ideas of blood pool contrast ultrasound imaging (first discovered by serendipity) [101] come from the use of air bubbles generated in saline, serum albumin solutions or viscous X-ray contrast media. Unlike water (or most of biological tissues), gas bubbles are very compressible; thus, in response to the passage of the ultrasound wave as the cycles of positive and negative pressure, microbubbles rapidly compress and expand about their equilibrium (ambient) pressure setting, with the particle diameter variation reaching several fold [102]; movement of gas-liquid interface creates secondary pressure waves, i.e., ultrasound scattering. Luckily for this field, relatively small bubbles, with the diameter somewhat less than of a red blood cell, can scatter MHz ultrasound very efficiently, and can be detected by ultrasound imaging, with excellent sensitivity. A single microbubble, with a sub-picogram mass, can be observed at multi-cm depth, with abundant clinical imaging systems, in real time (at 20–30 frames/s or faster) [103]. Thus, the dose of the administered ultrasound contrast material can be in the single milligram or sub-milligram range, of which most material is either fully natural (e.g., human serum albumin in Optison microbubbles [104], or synthetic fully biocompatible, such as phospholipids, e.g., in Definity [105] and Sonovue microbubbles [106]). Non-microbubble ultrasound contrast agents were tested widely at the preclinical stage, but have not yet made it to the clinical application level, perhaps due to the larger required dose and lower acoustic backscatter.

Ultrasound contrast is used as a general radiology intravascular agent worldwide (so far the USA is an exception, where only cardiac ultrasound contrast imaging is approved in the clinic). Worldwide, several million ultrasound contrast exams take place every year; due to the low dose of the contrast material, serious side effects are infrequent; for the patients with kidney impairment, where X-ray contrast or Gd-based MRI contrast agents are undesirable, microbubble contrast exam may become the preferred option [107].

In order to observe microbubble particles in the bloodstream, contrast-specific detection schemes and pulse sequences have been implemented, with multi-pulse detection schemes being the most efficient. A combination of phase inversion (i.e., compression-first and rarefaction-first pulses) and power modulation (i.e., pulses with varying ultrasound transmit amplitude) provides the best sensitivity to contrast along with an excellent suppression of the background tissue signal [108]; see accompanying video of microbubbles influx into the tumor vasculature in a murine model. Contrast mode is often used in combination with regular grayscale B-mode imaging for anatomy positioning (see Figure 4). It is important that microbubble detection in the tissues can be achieved at low acoustic power levels, i.e., without destroying the microbubbles.

Real-time ultrasound contrast imaging capability is often used for characterization of cancerous nodules: after an intravenous bolus injection, tissue arrival time for normal tissues, benign and malignant tumors may differ significantly [109]. Modern imaging equipment has a color-coded arrival time routine, which allows a distinct presentation of the contrast arrival time differential between the tumor and surrounding tissues.

Destruction-replenishment as a tool for perfusion contrast imaging

In the 1990s, at the time when microbubble detection was not as sensitive, the most efficient way to monitor microbubble contrast in the bloodstream was to destroy them by higher acoustic pressure of ultrasound. Typically, with mechanical index (MI) in excess of 0.3, and up to 1.9 (as allowed for the diagnostic imaging scanners) destruction is achieved within just one imaging frame. Therefore, taking advantage of this targeted microbubble destruction in the interrogated volume with intermittent timed frame collection, Kaul et al [110] devised a tool to monitor myocardial perfusion, with the aim to observe perfusion defects in heart muscle following myocardial infarction. Intermittent imaging was performed in synchrony with heart pulses, triggered by EKG, typically at end-systole. Following microbubble infusion, when microbubbles concentration in the vasculature reached a constant level, ultrasound imaging was initiated and performed at every heart beat, then at every other heartbeat, then every third, fourth and fifth heartbeat. Microbubbles from outside of the insonated field (typically, a thin slice, 1–5 mm thick and up to 5 −15 cm long and wide) start to refill the vasculature, larger arteries first, followed by arterioles, capillaries, postcapillary venules and veins. It has been suggested that by timing the interval of ultrasound pulses, the fraction of the blood in the particular portion of the vasculature (e.g., capillaries) can be estimated [111].

Lately, with the advent of high-sensitivity multipulse detection schemes, ultrasound contrast imaging does not require microbubble destruction anymore. Therefore, after a single destructive pulse, replenishment of microbubbles into the interrogated volume can be monitored in real time, with the traditional clinical imaging equipment at 20–50 frames per second [112], (see Figure 5 and accompanying video) and with the most modern equipment at 10^3 Hz or even faster [113, 114].

Overall, perfusion studies with microbubble contrast are now routinely used in the clinical setting worldwide (except USA as of now); they can provide blood flux information in the settings where Doppler imaging is not useful due to smallest size of the vessels in the tissue (e.g., in a transplanted skin flap [115]). An unfortunate limitation of this technique is in the inability of ultrasound at imaging frequencies to transit through the human skull without attenuation; thus, brain perfusion studies that are routinely performed with functional MRI cannot be performed with contrast ultrasound unless there is a burr hole present [116].

Molecular (Targeted) Contrast Ultrasound Imaging

Expanding the ability of ultrasound imaging to collect information on the biological processes at the molecular and cellular level requires the use of a specialized contrast agents, targeted microbubbles [117]. The general idea is traditional for targeted contrast imaging: a contrast particle is conjugated with the targeting ligand that possesses affinity towards the

disease marker. The particles are administered in vivo (e.g., intravenously), circulate in the body, and accumulate in the area of disease.

As the typical mean size of microbubble contrast agents is several micrometers, these agents are unable to probe the receptors located outside of the vascular bed. Although nanobubble studies have been repeatedly reported in the literature over the past decade [118, 119]), the acoustic backscatter and particle lifetime are both rather low and these agents have not approached practical application; therefore, ultrasound contrast imaging of leaky neovasculature (e.g., as in enhanced permeability and retention effect, EPR, [120]) is most likely going to be limited to the phase-shift liquid fluorocarbon nanodroplet formulations [121].

Current progress of molecular imaging with micrometer-sized targeted bubbles has been significant. It started with a model ultrasound imaging study in vitro, in petri dishes, avidin-biotin targeting [117], and progressed rapidly towards the use of cell cultures and antibody-mediated targeting [122], followed by in vivo studies. Several targets were investigated with significant detail: thrombi, markers of inflammation, and markers of angiogenesis.

The simplest targeted contrast agent is already in clinical use: Sonazoid (perflubutane) formulation is approved for liver imaging in Japan and South Korea [123]. Targeting specificity of this agent is based on its lipid shell composition, phosphatidylserine. This phospholipid is a natural marker of apoptosis and a powerful driver for the phagocytic uptake of apoptotic cells [124, 125], cell fragments and other particles [126] by the cells of reticuloendothelial system (RES) and any other phagocytic cells, e.g., leukocytes, specifically, neutrophils. The latter cell is the first to adhere to vascular endothelium in the acute inflammatory response to ischemia-reperfusion injury, e.g., in an experimental myocardial infarction [127], or in the acute kidney injury scenario [128], which allows targeted microbubble ultrasound imaging.

More specific endothelial markers of interest to microbubble targeting include selectins (P- and E-) and integrins, such as VCAM-1 and ICAM-1, which are expressed on the surface of vascular endothelium in response to inflammatory stimuli. Microbubble targeting of these molecules is achieved either via antibody placement on the bubble shell [129] or the use of smaller molecules, such as peptides [130], nanobodies [131] or carbohydrates [132]. The latter molecule, sialyl Lewis X (or A), is present on the business end of a natural leukocyte membrane protein P-selectin glycoprotein ligand −1 (PSGL-1), a ligand for P- and E-selectin, so it is suitable for microbubble targeting to the sites of inflammation [133, 134] and to activated platelets [135].

Another significant application area for microbubble targeting is tumor vasculature: specific markers of vascular endothelium in the areas of malignant tumors can be successfully imaged by ligand-carrying microbubbles. Initially an antibody against the tumor vasculature biomarker $\alpha_v\beta_3$ was applied [136], later followed by targeting with other ligand molecules, such as modified RGD peptides [137]. VEGF Receptor 2 is another important biomarker of the malignant tumor vasculature; this molecule is already a popular target for tumor detection with other imaging modalities [138] as well as with ultrasound molecular imaging,

via microbubbles decorated with anti-VEGFR2 antibodies, [139], or single-chain VEGF [140], which has been shown to achieve selective accumulation of microbubbles in the tumor neovasculature in a murine model (see Figure 6). A synthetic heterodimeric peptide combination was discovered as a smaller molecule combination tool for VEGFR2 targeting [141]. The latter microbubble formulation, BR55, is in the ongoing Phase 1/2clinical trial, (see NCT02142608). Prior to this, an early-phase BR55 clinical trial for prostate cancer patients with scheduled radical prostatectomy compared VEGFR2 histology with targeted ultrasound imaging. This early study suggested co-location of the tumor nodules by both methods [142]. Molecular ultrasound imaging may be used to assist with image-guided biopsy (e.g., in the breast and prostate cancer setting) and targeted therapeutic interventions.

Overall, a combination of targeted contrast ultrasound agents with the wide availability of contrast imaging modalities on the ultrasound imaging equipment may result in the use of ultrasound molecular imaging for targeted diagnostics, image-guided biopsy and therapy.

Ultrasound in therapy: thermal and mechanical

Focused ultrasound has been suggested as a therapeutic modality decades ago [143], although wider clinical use of this approach started much later [144]. Induction of local hyperthermia by focused ultrasound is based on localized energy deposition. MRI can serve as a tool for precise temperature monitoring in the target tissue, although ultrasound imaging is used for ultrasound therapy guidance in the clinic widely outside of US. Maintaining tissue temperature of ∼45°C for 30–60 minutes (or much higher temperatures, for just a few seconds) is sufficient to kill the cells in the focal zone. Ultrasound of 0.6–1 MHz frequency is often used; from many cm away, a focal zone with the size and shape of a grain of rice can be formed using a focused transducer [145]. KW power of the therapeutic apparatus can achieve the desired temperature in the focal zone within seconds. Multi-element arrays (optimally, with thousands of elements) allow rapid electronic steering of the focal spot to accelerate the procedure and completely cover the desired treatment zone [146]. Approved indications include uterine fibroid therapy [147] and palliative treatment of bone metastases [148]. Lower frequency ultrasound (220 KHz, necessary for penetrating human skull without heating it significantly) is now being investigated as a tool for ultrasound therapy in the brain [149]. Focused ultrasound heating is now being tested as a non-invasive replacement of neurosurgical/electrode placement approach for treatment of essential tremor [150]. We can hope that tumor therapy will be successful in clinical trials in the bone metastasis setting (beyond palliation), as well as for treatment of brain tumors (e.g., NCT01698437) or prostate cancer (e.g., NCT02265159). Success of this non-invasive therapeutic modality is supported by the ability to focus ultrasound tightly and rapidly deep within the body (even through the skull). Limitations are also based on physical constraints: ultrasound energy is attenuated and absorbed by the bones (thus, brain treatment requires an additional CT or MRI study to adjust the ultrasound pulse sequences to compensate for the shape and thickness of the skull). Ultrasound cannot efficiently travel through the gas phase, so lung treatment can only be performed for liquid-filled lungs [151]. In some instances, ribcage obscures access to the target (e.g., certain areas of the liver). There have been reports that ribs in the way of ultrasound beam had been resected prior to the treatment with a large aperture single element transducer [152]. However, more appropriate would be to use multi-

element array and adjust the transmit power for the elements which are obscured by the ribs [153].

Histotripsy implies high-power pulverization of the tissues: a water fountain generated on the air-water interface in the focal zone of an ultrasound transducer is recreated by cavitation in vivo within the therapeutic target tissues, if peak negative acoustic pressure reaches 10 MPa [154]. Following this treatment, a void in the biological tissue is created: target tissue (e.g., tumor nodule) is destroyed to subcellular level and liquefied [155].

Thrombolysis with ultrasound

Enhancing the rate of thrombolysis with ultrasound has been suggested more than a decade ago [156, 157]. The idea is quite similar to tissue ablation, as described in the previous section; the acoustic energy applied for thrombolysis may be significantly lower, often within the limits of diagnostic ultrasound imaging. Ultrasound pressure wave provides mechanical action on the biological tissues (including the clot and surrounding blood). Liquid media streaming improves convection of the participants of the thrombolytic cascade in proximity and within the clot structure, resulting in thrombolysis acceleration. Presence of even small doses of thrombolytic agents and/or microbubbles (micro-foci of energy deposition and microstreaming) further accelerates thrombolysis. We can hope that ultrasound-assisted thrombolysis, if applied quickly (e.g., in an ambulance setting) will aid in reduction of the clot size, which in turn may help save brain tissue following stroke or myocardium following myocardial infarction [158]. Ultrasound can be applied non-invasively [159], or via a catheter [160].

Ultrasound-microbubble combination as a tool for targeted drug and gene delivery

Ultrasound has been investigated as a tool for microbubble-assisted drug delivery for almost two decades. Initially [161] model drugs were incorporated into the bubble shell. Later, tumor therapy in response to insonation was achieved in animal models [162, 163] - but that was feasible mostly for rather hydrophobic drugs, e.g., paclitaxel. Plasmid DNA could be attached onto the bubble shell electrostatically, and ultrasound-assisted transfection enhancement was observed with such constructs [164]. Attachment of drug-loaded liposomes onto the surface of microbubbles allows ultrasound-triggered drug delivery capability: in response to microbubble insonation the drug is released from the liposome core [165]. This has been shown to work with widely used anticancer drugs, e.g., doxorubicin [166] and paclitaxel [167].

A combination approach, where existing drug is simply co-administered along with clinical grade approved microbubbles and focused ultrasound, will obviously get to clinical trials faster. In this approach, stable cavitation of microbubbles within the vasculature is used to transiently alter permeability of blood-brain barrier [168]. The disruption of the barrier is mild and transient (permeability enhancement ceases within hours). However, large items, such as liposomes [169] and other nanoparticles [170] can be delivered into the brain tissue as efficiently as smaller items, such as antibodies [171], other drugs [172], or even Gd-based

MRI contrast agents [173] (See Figure 7 as an example of penetration enhancement of Gd-DTPA across blood-brain barrier in a rat model). This approach has already led to an exciting demonstration of glioma treatment in a rodent model (curative in a significant fraction of animals) with a simple combination of long-circulating doxorubicin liposomes (doxil) and clinical perflutren microbubbles [174]. Success of therapy can be explained by the ability of PEG-coated liposomes to stay in the bloodstream for many hours, recirculate through the insonated area vasculature and extravasate for many hours, as long as the drug remains in the bloodstream and the barrier remains open. Expansion of this technique towards clinical applications could be predicted, ranging from tumor therapy [174] to Alzheimer treatment [175, 176].

Similar therapeutic approach can be applied in the situations other than the blood-brain barrier, to any endothelial lining in the vasculature that precludes entry of the drug into the diseased tissue. This approach has been applied to deliver particles of adeno-associated virus to the insonated myocardium [177], as well as for the treatment of pancreatic cancer in an orthotopic xenograft mouse model, by a combination of anticancer drug gemcitabine and Sonovue microbubbles [178]. The latter combination has demonstrated interesting data in a clinical trial setting, initially showing the suppression of tumor growth in response to intravenous administration of gemcitabine, immediately followed by injections of Sonovue microbubbles every 3.5 min and continuous insonation of the primary tumor with an ultrasound imaging system during the next half hour [179], with repeated ultrasound/microbubble treatment cycles administered with every scheduled administration of gemcitabine, up to 32 weeks. Expansion of this trial to a larger group of patients now points towards the beneficial extension of life for the patients undergoing this treatment, with 60% surviving 12 months [180].

Bioeffects of ultrasound in therapeutic applications

Therapeutic applications of ultrasound may span beyond thermal or mechanical disruption of the tissues or drug delivery. Action of ultrasound on the tissues, possibly in combination with microbubbles, may lead to manifestation of a variety of therapeutic bioeffects, spanning from therapeutic angiogenesis [181] to inhibiting blood flow in the tumors [182–184], to targeting therapeutic stem cells following intravenous administration [185], bone fracture healing [186], and, surprisingly, ultrasound action on splenic nerve to mitigate acute kidney injury [187, 188]. Non-invasive brain stimulation by ultrasound is also quite intriguing [189].

All these techniques are based on the ability of ultrasound (as a pressure wave) to provide guided energy deposition in the treatment area; in some instances the ultrasound action is further enhanced by the presence of vibrating microbubbles. Physiological effects demonstrated by ultrasound application are quite diverse and will definitely lead to the development of new therapeutic approaches and modalities.

Conclusion

Ultrasound has become an indispensable tool of modern medicine that helps expand the borders of radiology. Hardware improvements, based on continuous acceleration of data processing rate, lower cost and smaller size of the electronic devices, are combined with smart transducer design, pulse sequences and novel data processing and analysis schemes. Hand-held and laptop ultrasound is already in wide use, soon to replace cart-based systems. Ultrasound contrast agents bring the ability to monitor tissue perfusion, and targeted agents enable molecular ultrasound imaging of the vascular biomarkers of angiogenesis or inflammation. The ability to direct ultrasound to the desired areas of the body opens up direct therapeutic applications of this modality, including targeted drug and gene delivery, and thrombolytic therapy enhancement. Overall, ultrasound is rapidly developing both as an imaging and a therapeutic modality.

Acknowledgments

Support:

NIH EB016752, EB001826, EB002349, HL090700, HL111077, CA102880, DK093841.

REFERENCES

1. Szabo, T. ISBN: 9780123964878. 2nd Edition. Elsevier; 2013. Diagnostic Ultrasound Imaging: Inside Out.
2. Moore G. Cramming More Components onto Integrated Circuits. Electronics. 1965:114–117.
3. Tanter M, Fink M. Ultrafast Imaging in Biomedical Ultrasound. IEEE Transactions on Ultrasonics Ferroelectrics and Frequency Control. 2014; 61:102–119.
4. Schneider FK, Agarwal A, Yoo YM, et al. A Fully Programmable Computing Architecture for Medical Ultrasound Machines. Ieee Transactions on Information Technology in Biomedicine. 2010; 14:538–540. [PubMed: 19546045]
5. Blaivas M, Brannam L, Theodoro D. Ultrasound image quality comparison between an inexpensive handheld emergency department (ED) ultrasound machine and a large mobile ED ultrasound system. Academic Emergency Medicine. 2004; 11:778–781. [PubMed: 15231471]
6. Lamperti M, Bodenham AR, Pittiruti M, et al. International evidence-based recommendations on ultrasound-guided vascular access. Intensive Care Medicine. 2012; 38:1105–1117. [PubMed: 22614241]
7. Atar S, Feldman A, Darawshe A, et al. Utility and diagnostic accuracy of hand-carried ultrasound for emergency room evaluation of chest pain. American Journal of Cardiology. 2004; 94:408–409. [PubMed: 15276122]
8. Callegari L, Leonardi A, Bini A, et al. Ultrasound-guided removal of foreign bodies: personal experience. European Radiology. 2009; 19:1273–1279. [PubMed: 19153745]
9. Sargsyan AE, Hamilton DR, Jones JA, et al. FAST at MACH 20: clinical ultrasound aboard the International Space Station. The Journal of trauma. 2005; 58:35–39. [PubMed: 15674147]
10. Nations JA, Browning RF. Battlefield applications for handheld ultrasound. Ultrasound quarterly. 2011; 27:171–176. [PubMed: 21873854]
11. Wells, P. Biomedical Ultrasonics. 1st ed.. New York, NY: Academic Publishing; 1977.
12. Mast TD, Hinkelman LM, Orr MJ, et al. Simulation of ultrasonic pulse propagation through the abdominal wall. The Journal of the Acoustical Society of America. 1997; 102:1177–1190. [PubMed: 9265762]
13. Flax SW, O'Donnell M. Phase-aberration correction using signals from point reflectors and diffuse scatterers: basic principles. IEEE transactions on ultrasonics, ferroelectrics, and frequency control. 1988; 35:758–767.

14. Liu DL, Waag RC. A Comparison of Ultrasonic Wave-Front Distortion and Compensation in One-Dimensional and 2-Dimensional Apertures. IEEE Transactions on Ultrasonics Ferroelectrics and Frequency Control. 1995; 42:726–733.
15. Wildes DG, Chiao RY, Daft CMW, et al. Elevation performance of 1.25D and 1.5D transducer arrays. IEEE Transactions on Ultrasonics Ferroelectrics and Frequency Control. 1997; 44:1027–1037.
16. Liu DL, Waag RC. Correction of Ultrasonic Wave-Front Distortion Using Backpropagation and a Reference Wave-Form Method for Time-Shift Compensation. J Acoust Soc Am. 1994; 96:649–660. [PubMed: 7930065]
17. Fink M. Time-Reversal of Ultrasonic Fields. 1. Basic Principles. IEEE Transactions on Ultrasonics Ferroelectrics and Frequency Control. 1992; 39:555–566.
18. Pernot M, Montaldo G, Tanter M, et al. "Ultrasonic stars" for time-reversal focusing using induced cavitation bubbles. Appl Phys Lett. 2006; 88:034102.
19. Li PC, Li ML. Adaptive imaging using the generalized coherence factor. IEEE Transactions on Ultrasonics Ferroelectrics and Frequency Control. 2003; 50:128–141.
20. Clement GT, Hynynen K. Micro-receiver guided transcranial beam steering. IEEE Transactions on Ultrasonics Ferroelectrics and Frequency Control. 2002; 49:447–453.
21. Aubry JF, Tanter M, Pernot M, et al. Experimental demonstration of noninvasive transskull adaptive focusing based on prior computed tomography scans. J Acoust Soc Am. 2003; 113:84–93. [PubMed: 12558249]
22. Haworth KJ, Fowlkes JB, Carson PL, et al. Towards aberration correction of transcranial ultrasound using acoustic droplet vaporization. Ultrasound Med Biol. 2008; 34:435–445. [PubMed: 17935872]
23. Vyas U, Kaye E, Pauly KB. Transcranial phase aberration correction using beam simulations and MR- ARFI. Med Phys. 2014; 41:032901. [PubMed: 24593740]
24. Christopher T. Finite amplitude distortion-based inhomogeneous pulse echo ultrasonic imaging. IEEE Transactions on Ultrasonics Ferroelectrics and Frequency Control. 1997; 44:125–139.
25. Dahl JJ, Jakovljevic M, Pinton GF, et al. Harmonic Spatial Coherence Imaging: An Ultrasonic Imaging Method Based on Backscatter Coherence. IEEE transactions on ultrasonics, ferroelectrics, and frequency control. 2012; 59:648–659.
26. Spencer KT, Bednarz J, Rafter PG, et al. Use of harmonic imaging without echocardiographic contrast to improve two-dimensional image quality. The American journal of cardiology. 1998; 82:794–799. [PubMed: 9761093]
27. Tranquart F, Grenier N, Eder V, et al. Clinical use of ultrasound tissue harmonic imaging. Ultrasound Med Biol. 1999; 25:889–894. [PubMed: 10461715]
28. Pinton GF, Trahey GE, Dahl JJ. Sources of Image Degradation in Fundamental and Harmonic Ultrasound Imaging: A Nonlinear, Full-Wave, Simulation Study (vol 58, pg 754, 2011). IEEE Transactions on Ultrasonics Ferroelectrics and Frequency Control. 2011; 58:1272–1283.
29. Kass M, Witkin A, Terzopoulos D. Snakes: Active contour models. Int J Comput Vision. 1988; 1:321–331.
30. Caselles V, Kimmel R, Sapiro G. Geodesic active contours. Int J Comput Vision. 1997; 22:61–79.
31. Loizou CP, Pattichis CS, Pantziaris M, et al. Snakes based segmentation of the common carotid artery intima media. Medical & Biological Engineering & Computing. 2007; 45:35–49. [PubMed: 17203319]
32. Yu YJ, Molloy JA, Acton ST. Segmentation of the prostate from suprapubic ultrasound images. Med Phys. 2004; 31:3474–3484. [PubMed: 15651630]
33. Abd-Elmoniem KZ, Youssef ABM, Kadah YM. Real-time speckle reduction and coherence enhancement in ultrasound imaging via nonlinear anisotropic diffusion. Ieee Transactions on Biomedical Engineering. 2002; 49:997–1014. [PubMed: 12214889]
34. Bamber JC, Daft C. Adaptive filtering for reduction of speckle in ultrasonic pulse-echo images. Ultrasonics. 1986; 24:41–44. [PubMed: 3510500]
35. Dutt V, Greenleaf JF. Adaptive speckle reduction filter for log-compressed B-scan images. IEEE Transactions on Medical Imaging. 1996; 15:802–813. [PubMed: 18215960]

36. Michailovich OV, Tannenbaum A. Despeckling of medical ultrasound images. IEEE Transactions on Ultrasonics Ferroelectrics and Frequency Control. 2006; 53:64–78.
37. Yu YJ, Acton ST. Speckle reducing anisotropic diffusion. IEEE Transactions on Image Processing. 2002; 11:1260–1270. [PubMed: 18249696]
38. Zong XL, Laine AF, Geiser EA. Speckle reduction and contrast enhancement of echocardiograms via multiscale nonlinear processing. IEEE Transactions on Medical Imaging. 1998; 17:532–540. [PubMed: 9845309]
39. Sun QL, Hossack JA, Tang JS, et al. Speckle reducing anisotropic diffusion for 3D ultrasound images. Computerized Medical Imaging and Graphics. 2004; 28:461–470. [PubMed: 15541953]
40. Chen C-M, Lu HH-S, Lin Y-C. An early vision-based snake model for ultrasound image segmentation. Ultrasound in Medicine & Biology. 2000; 26:273–285. [PubMed: 10722917]
41. Chen D-R, Chang R-F, Wu W-J, et al. 3-D breast ultrasound segmentation using active contour model. Ultrasound in Medicine & Biology. 2003; 29:1017–1026. [PubMed: 12878248]
42. Chang RF, Wu WJ, Tseng CC, et al. 3-D Snake for US in Margin Evaluation for Malignant Breast Tumor Excision Using Mammotome. Ieee Transactions on Information Technology in Biomedicine. 2003; 7:197–201. [PubMed: 14518733]
43. Entrekin RR, Porter BA, Sillesen HH, et al. Real-time spatial compound imaging: Application to breast, vascular, and musculoskeletal ultrasound. Seminars in Ultrasound Ct and Mri. 2001; 22:50–64.
44. Huber S, Wagner M, Medl M, et al. Real-time spatial compound imaging in breast ultrasound. Ultrasound Med Biol. 2002; 28:155–163. [PubMed: 11937277]
45. Lediju MA, Pihl MJ, Hsu SJ, et al. A Motion-Based Approach to Abdominal Clutter Reduction. IEEE Transactions on Ultrasonics Ferroelectrics and Frequency Control. 2009; 56:2437–2449.
46. Zwirn G, Akselrod S. Stationary clutter rejection in echocardiography. Ultrasound in Medicine & Biology. 2006; 32:43–52. [PubMed: 16364796]
47. Mauldin FW, Lin D, Hossack JA. The Singular Value Filter: A General Filter Design Strategy for PCA-Based Signal Separation in Medical Ultrasound Imaging. IEEE Transactions on Medical Imaging. 2011; 30:1951–1964. [PubMed: 21693416]
48. Delgado V, Ypenburg C, van Bommel RJ, et al. Assessment of left ventricular dyssynchrony by speckle tracking strain imaging - Comparison between longitudinal, circumferential, and radial strain in cardiac resynchronization therapy. Journal of the American College of Cardiology. 2008; 51:1944–1952. [PubMed: 18482662]
49. Nesser H-J, Mor-Avi V, Gorissen W, et al. Quantification of left ventricular volumes using three-dimensional echocardiographic speckle tracking: comparison with MRI. European Heart Journal. 2009; 30:1565–1573. [PubMed: 19482868]
50. Notomi Y, Lysyansky P, Setser RM, et al. Measurement of ventricular torsion by two-dimensional ultrasound speckle tracking imaging. Journal of the American College of Cardiology. 2005; 45:2034–2041. [PubMed: 15963406]
51. Golemati S, Sassano A, Lever MJ, et al. Carotid artery wall motion estimated from B-mode ultrasound using region tracking and block matching. Ultrasound Med Biol. 2003; 29:387–389. [PubMed: 12706190]
52. Kasai C, Namekawa K, Koyano A, et al. Real-Time Two-Dimensional Blood Flow Imaging Using an Autocorrelation Technique. Sonics and Ultrasonics, IEEE Transactions on. 1985; 32:458–464.
53. Loupas T, Powers JT, Gill RW. An axial velocity estimator for ultrasound blood flow imaging, based on a full evaluation of the Doppler equation by means of a two-dimensional autocorrelation approach. IEEE Transactions on Ultrasonics, Ferroelectrics, and Frequency Control. 1995; 42:672–688.
54. Bonnefous O, Pesqué P. Time domain formulation of pulse-Doppler ultrasound and blood velocity estimation by cross correlation. Ultrasonic Imaging. 1986; 8:73–85. [PubMed: 2946098]
55. Trahey GE, Allison JW, von Ramm OT. Angle independent ultrasonic detection of blood flow. IEEE transactions on bio-medical engineering. 1987; 34:965–967. [PubMed: 2961682]
56. Jensen JA, Munk P. A new method for estimation of velocity vectors. IEEE Transactions on Ultrasonics Ferroelectrics and Frequency Control. 1998; 45:837–851.

57. Anderson ME. Multi-dimensional velocity estimation with ultrasound using spatial quadrature. IEEE Transactions on Ultrasonics Ferroelectrics and Frequency Control. 1998; 45:852–861.
58. Jensen JA. A new estimator for vector velocity estimation. IEEE Transactions on Ultrasonics Ferroelectrics and Frequency Control. 2001; 48:886–894.
59. Nikolov ST, Jensen JA. In-vivo synthetic aperture flow imaging in medical ultrasound. IEEE Transactions on Ultrasonics Ferroelectrics and Frequency Control. 2003; 50:848–856.
60. Udesen J, Gran F, Hansen KL, et al. High frame-rate blood vector velocity imaging using plane waves: Simulations and preliminary experiments. IEEE Transactions on Ultrasonics Ferroelectrics and Frequency Control. 2008; 55:1729–1743.
61. Bercoff J, Montaldo G, Loupas T, et al. Ultrafast Compound Doppler Imaging: Providing Full Blood Flow Characterization. IEEE Transactions on Ultrasonics Ferroelectrics and Frequency Control. 2011; 58:134–147.
62. Nissen SE, Yock P. Intravascular Ultrasound: Novel Pathophysiological Insights and Current Clinical Applications. Circulation. 2001; 103:604–616. [PubMed: 11157729]
63. Fercher AF, Drexler W, Hitzenberger CK, et al. Optical coherence tomography - principles and applications. Reports on Progress in Physics. 2003; 66:239–303.
64. Kodach VM, Kalkman J, Faber DJ, et al. Quantitative comparison of the OCT imaging depth at 1300 nm and 1600 nm. Biomed Opt Express. 2010; 1:176–185. [PubMed: 21258456]
65. Sethuraman S, Aglyamov SR, Amirian JH, et al. Intravascular photoacoustic imaging using an IVUS imaging catheter. IEEE Transactions on Ultrasonics Ferroelectrics and Frequency Control. 2007; 54:978–986.
66. Sethuraman S, Amirian JH, Litovsky SH, et al. Spectroscopic intravascular photoacoustic imaging to differentiate atherosclerotic plaques. Optics Express. 2008; 16:3362–3367. [PubMed: 18542427]
67. Wang B, Su JL, Amirian J, et al. Detection of lipid in atherosclerotic vessels using ultrasound-guided spectroscopic intravascular photoacoustic imaging. Optics Express. 2010; 18:4889–4897. [PubMed: 20389501]
68. Jansen K, van der Steen AFW, Wu M, et al. Spectroscopic intravascular photoacoustic imaging of lipids in atherosclerosis. Journal of Biomedical Optics. 2014; 19:26006-1–26006-9.
69. Emelianov SY, Pai-Chi L, O'Donnell M. Photoacoustics for molecular imaging and therapy. Physics Today. 2009; 62:34–39. [PubMed: 20523758]
70. Ophir J, Cespedes I, Ponnekanti H, et al. Elastography - a quantitative method for imaging the elasticity of biological tissues. Ultrasonic Imaging. 1991; 13:111–134. [PubMed: 1858217]
71. Odonnell M, Skovoroda AR, Shapo BM, et al. Internal displacement and strain imaging using ultrasonic speckle tracking. IEEE Transactions on Ultrasonics Ferroelectrics and Frequency Control. 1994; 41:314–325.
72. Cespedes I, Huang Y, Ophir J, et al. Methods for estimation of subsample time delays of digitized echo signals. Ultrasonic Imaging. 1995; 17:142–171. [PubMed: 7571208]
73. Cespedes I, Ophir J. Reduction of image noise in elastography. Ultrasonic Imaging. 1993; 15:89–102. [PubMed: 8346613]
74. Konofagou E, Ophir J. A new elastographic method for estimation and imaging of lateral displacements, lateral strains, corrected axial strains and Poisson's ratios in tissues. Ultrasound Med Biol. 1998; 24:1183–1199. [PubMed: 9833588]
75. Lubinski MA, Emelianov SY, O'Donnell M. Speckle tracking methods for ultrasonic elasticity imaging using short-time correlation. IEEE Transactions on Ultrasonics Ferroelectrics and Frequency Control. 1999; 46:82–96.
76. Lubinski MA, Emelianov SY, O'Donnell M. Adaptive strain estimation using retrospective processing. IEEE Transactions on Ultrasonics Ferroelectrics and Frequency Control. 1999; 46:97–107.
77. Skovoroda AR, Lubinski MA, Emelianov SY, et al. Reconstructive elasticity imaging for large deformations. IEEE Transactions on Ultrasonics Ferroelectrics and Frequency Control. 1999; 46:523–535.
78. Garra BS, Cespedes EI, Ophir J, et al. Elastography of breast lesions: Initial clinical results. Radiology. 1997; 202:79–86. [PubMed: 8988195]

79. Itoh A, Ueno E, Tohno E, et al. Breast disease: Clinical application of US elastography for diagnosis. Radiology. 2006; 239:341–350. [PubMed: 16484352]
80. Cochlin DL, Ganatra RH, Griffiths DFR. Elastography in the Detection of Prostatic Cancer. Clinical Radiology. 2002; 57:1014–1020. [PubMed: 12409113]
81. Lyshchik A, Higashi T, Asato R, et al. Thyroid gland tumor diagnosis at US elastography. Radiology. 2005; 237:202–211. [PubMed: 16118150]
82. Cespedes EI, de Korte CL, van der Steen AF, et al. Intravascular elastography: principles and potentials. Seminars in interventional cardiology : SIIC. 1997; 2:55–62. [PubMed: 9546985]
83. de Korte CL, Carlier SG, Mastik F, et al. Morphological and mechanical information of coronary arteries obtained with intravascular elastography - Feasibility study in vivo. European Heart Journal. 2002; 23:405–413. [PubMed: 11846498]
84. de Korte CL, van der Steen AFW, Cespedes EI, et al. Intravascular ultrasound elastography in human arteries: Initial experience in vitro. Ultrasound Med Biol. 1998; 24:401–408. [PubMed: 9587995]
85. Fahey BJ, Nightingale KR, Nelson RC, et al. Acoustic radiation force impulse imaging of the abdomen: Demonstration of feasibility and utility. Ultrasound Med Biol. 2005; 31:1185–1198. [PubMed: 16176786]
86. Nightingale K, Soo MS, Nightingale R, et al. Acoustic radiation force impulse imaging: In vivo demonstration of clinical feasibility. Ultrasound Med Biol. 2002; 28:227–235. [PubMed: 11937286]
87. Trahey GE, Palmeri ML, Bentley RC, et al. Acoustic radiation force impulse imaging of the mechanical properties of arteries: In vivo and ex vivo results. Ultrasound Med Biol. 2004; 30:1163–1171. [PubMed: 15550320]
88. Jaffer OS, Lung PFC, Bosanac D, et al. Acoustic radiation force impulse quantification: repeatability of measurements in selected liver segments and influence of age, body mass index and liver capsule-to-box distance. The British Journal of Radiology. 2012; 85:e858–e863. [PubMed: 22763032]
89. Bercoff J, Tanter M, Fink M. Supersonic shear imaging: A new technique for soft tissue elasticity mapping. IEEE Transactions on Ultrasonics Ferroelectrics and Frequency Control. 2004; 51:396–409.
90. Tanter M, Bercoff J, Athanasiou A, et al. Quantitative assessment of breast lesion viscoelasticity: Initial clinical results using supersonic shear imaging. Ultrasound Med Biol. 2008; 34:1373–1386. [PubMed: 18395961]
91. Xu MH, Wang LHV. Photoacoustic imaging in biomedicine. Review of Scientific Instruments. 2006; 77:041101-1–041101-22.
92. Wang LV. Prospects of photoacoustic tomography. Med Phys. 2008; 35:5758–5767. [PubMed: 19175133]
93. Li C, Wang LV. Photoacoustic tomography and sensing in biomedicine. Physics in Medicine and Biology. 2009; 54:R59–R97. [PubMed: 19724102]
94. Wang LV. Multiscale photoacoustic microscopy and computed tomography. Nature Photonics. 2009; 3:503–509. [PubMed: 20161535]
95. Xu Y, Wang LV, Ambartsoumian G, et al. Reconstructions in limited-view thermoacoustic tomography. Med Phys. 2004; 31:724–733. [PubMed: 15124989]
96. Gamelin J, Maurudis A, Aguirre A, et al. A real-time photoacoustic tomography system for small animals. Optics Express. 2009; 17:10489–10498. [PubMed: 19550444]
97. iTheraMedical. [(accessed April 01, 2015)] http://www.ithera-medical.com/technology/preclinical-systems.html.
98. Jansen K, van der Steen AFW, van Beusekom HMM, et al. Intravascular photoacoustic imaging of human coronary atherosclerosis. Optics Letters. 2011; 36:597–599. [PubMed: 21368919]
99. Zhang EZ, Povazay B, Laufer J, et al. Multimodal photoacoustic and optical coherence tomography scanner using an all optical detection scheme for 3D morphological skin imaging. Biomed Opt Express. 2011; 2:2202–2215. [PubMed: 21833358]
100. Hu S, Wang L. Photoacoustic Tomography: In Vivo Imaging from Organelles to Organs. Science. 2012; 335:1458–1462. [PubMed: 22442475]

101. Gramiak R, Shah PM. Echocardiography of the aortic root. Investigative radiology. 1968; 3:356–366. [PubMed: 5688346]
102. Chomas JE, Dayton PA, May D, et al. Optical observation of contrast agent destruction. Appl Phys Lett. 2000; 77:1056–1058.
103. Klibanov AL, Rasche PT, Hughes MS, et al. Detection of individual microbubbles of ultrasound contrast agents: imaging of free-floating and targeted bubbles. Investigative radiology. 2004; 39:187–195. [PubMed: 15076011]
104. Skyba DM, Camarano G, Goodman NC, et al. Hemodynamic characteristics, myocardial kinetics and microvascular rheology of FS-069, a second-generation echocardiographic contrast agent capable of producing myocardial opacification from a venous injection. J Am Coll Cardiol. 1996; 28:1292–1300. [PubMed: 8890829]
105. Fritz T, McKeon M, Unger E. Preclinical studies of MRX-115: safety evaluations of a myocardial perfusion agent. Academic radiology. 1996; 3(Suppl 2):S185–S187. [PubMed: 8796557]
106. Schneider M, Arditi M, Barrau MB, et al. BR1: a new ultrasonographic contrast agent based on sulfur hexafluoride-filled microbubbles. Investigative radiology. 1995; 30:451–457. [PubMed: 8557510]
107. Kalantarinia K, Belcik JT, Patrie JT, et al. Real-time measurement of renal blood flow in healthy subjects using contrast-enhanced ultrasound. American journal of physiology, Renal physiology. 2009; 297:F1129–F1134. [PubMed: 19625375]
108. Phillips P, Gardner E. Contrast-agent detection and quantification. Eur Radiol. 2004; 14(Suppl 8):P4–P10. [PubMed: 15700327]
109. Pitre-Champagnat S, Leguerney I, Bosq J, et al. Dynamic contrast-enhanced ultrasound parametric maps to evaluate intratumoral vascularization. Investigative radiology. 2015; 50:212–217. [PubMed: 25275834]
110. Wei K, Jayaweera AR, Firoozan S, et al. Quantification of myocardial blood flow with ultrasound-induced destruction of microbubbles administered as a constant venous infusion. Circulation. 1998; 97:473–483. [PubMed: 9490243]
111. Coggins M, Lindner J, Rattigan S, et al. Physiologic hyperinsulinemia enhances human skeletal muscle perfusion by capillary recruitment. Diabetes. 2001; 50:2682–2690. [PubMed: 11723050]
112. Dietrich CF, Averkiou MA, Correas JM, et al. An EFSUMB introduction into Dynamic Contrast-Enhanced Ultrasound (DCE-US) for quantification of tumour perfusion. Ultraschall Med. 2012; 33:344–351. [PubMed: 22843433]
113. Couture O, Bannouf S, Montaldo G, et al. Ultrafast imaging of ultrasound contrast agents. Ultrasound Med Biol. 2009; 35:1908–1916. [PubMed: 19699026]
114. Yiu BY, Yu AC. High-frame-rate ultrasound color-encoded speckle imaging of complex flow dynamics. Ultrasound Med Biol. 2013; 39:1015–1025. [PubMed: 23511009]
115. Christiansen JP, Leong-Poi H, Amiss LR, et al. Skin perfusion assessed by contrast ultrasound predicts tissue survival in a free flap model. Ultrasound Med Biol. 2002; 28:315–320. [PubMed: 11978411]
116. Rim SJ, Leong-Poi H, Lindner JR, et al. Quantification of cerebral perfusion with “Real-Time” contrast-enhanced ultrasound. Circulation. 2001; 104:2582–2587. [PubMed: 11714654]
117. Klibanov AL, Hughes MS, Marsh JN, et al. Targeting of ultrasound contrast material. An in vitro feasibility study. Acta radiologica Suppl. 1997; 412:113–120.
118. Wu H, Rognin NG, Krupka TM, et al. Acoustic characterization and pharmacokinetic analyses of new nanobubble ultrasound contrast agents. Ultrasound Med Biol. 2013; 39:2137–2146. [PubMed: 23932272]
119. Patel D, Dayton P, Gut J, et al. Optical and acoustical interrogation of submicron contrast agents. IEEE transactions on ultrasonics, ferroelectrics, and frequency control. 2002; 49:1641–1651.
120. Matsumura Y, Maeda H. A new concept for macromolecular therapeutics in cancer chemotherapy: mechanism of tumoritropic accumulation of proteins and the antitumor agent smancs. Cancer research. 1986; 46:6387–6392. [PubMed: 2946403]
121. Phillips LC, Puett C, Sheeran PS, et al. Phase-shift perfluorocarbon agents enhance high intensity focused ultrasound thermal delivery with reduced near-field heating. J Acoust Soc Am. 2013; 134:1473–1482. [PubMed: 23927187]

122. Villanueva FS, Jankowski RJ, Klibanov S, et al. Microbubbles targeted to intercellular adhesion molecule-1 bind to activated coronary artery endothelial cells. Circulation. 1998; 98:1–5. [PubMed: 9665051]

123. Forsberg F, Piccoli CW, Liu JB, et al. Hepatic tumor detection: MR imaging and conventional US versus pulse-inversion harmonic US of NC100100 during its reticuloendothelial system-specific phase. Radiology. 2002; 222:824–829. [PubMed: 11867808]

124. Schroit AJ, Madsen JW, Tanaka Y. In vivo recognition and clearance of red blood cells containing phosphatidylserine in their plasma membranes. The Journal of biological chemistry. 1985; 260:5131–5138. [PubMed: 3988747]

125. Allen TM, Williamson P, Schlegel RA. Phosphatidylserine as a determinant of reticuloendothelial recognition of liposome models of the erythrocyte surface. Proceedings of the National Academy of Sciences of the United States of America. 1988; 85:8067–8071. [PubMed: 3186707]

126. Fadok VA, Voelker DR, Campbell PA, et al. Exposure of phosphatidylserine on the surface of apoptotic lymphocytes triggers specific recognition and removal by macrophages. J Immunol. 1992; 148:2207–2216. [PubMed: 1545126]

127. Christiansen JP, Leong-Poi H, Klibanov AL, et al. Noninvasive imaging of myocardial reperfusion injury using leukocyte-targeted contrast echocardiography. Circulation. 2002; 105:1764–1767. [PubMed: 11956115]

128. Lindner JR, Song J, Xu F, et al. Noninvasive ultrasound imaging of inflammation using microbubbles targeted to activated leukocytes. Circulation. 2000; 102:2745–2750. [PubMed: 11094042]

129. Lindner JR, Song J, Christiansen J, et al. Ultrasound assessment of inflammation and renal tissue injury with microbubbles targeted to P-selectin. Circulation. 2001; 104:2107–2112. [PubMed: 11673354]

130. Schumann PA, Christiansen JP, Quigley RM, et al. Targeted-microbubble binding selectively to GPIIb IIIa receptors of platelet thrombi. Investigative radiology. 2002; 37:587–593. [PubMed: 12393970]

131. Hernot S, Unnikrishnan S, Du Z, et al. Nanobody-coupled microbubbles as novel molecular tracer. Journal of controlled release. 2012; 158:346–353. [PubMed: 22197777]

132. Weller GE, Villanueva FS, Tom EM, et al. Targeted ultrasound contrast agents: in vitro assessment of endothelial dysfunction and multi-targeting to ICAM-1 and sialyl Lewisx. Biotechnology and bioengineering. 2005; 92:780–788. [PubMed: 16121392]

133. Klibanov AL, Rychak JJ, Yang WC, et al. Targeted ultrasound contrast agent for molecular imaging of inflammation in high-shear flow. Contrast media & molecular imaging. 2006; 1:259–266. [PubMed: 17191766]

134. Rychak JJ, Li B, Acton ST, et al. Selectin ligands promote ultrasound contrast agent adhesion under shear flow. Molecular pharmaceutics. 2006; 3:516–524. [PubMed: 17009850]

135. Guenther F, von zur Muhlen C, Ferrante EA, et al. An ultrasound contrast agent targeted to P-selectin detects activated platelets at supra-arterial shear flow conditions. Investigative radiology. 2010; 45:586–591. [PubMed: 20808239]

136. Ellegala DB, Leong-Poi H, Carpenter JE, et al. Imaging tumor angiogenesis with contrast ultrasound and microbubbles targeted to alpha(v)beta3. Circulation. 2003; 108:336–341. [PubMed: 12835208]

137. Dayton PA, Pearson D, Clark J, et al. Ultrasonic analysis of peptide- and antibody-targeted microbubble contrast agents for molecular imaging of alphavbeta3-expressing cells. Molecular imaging. 2004; 3:125–134. [PubMed: 15296677]

138. Backer MV, Levashova Z, Patel V, et al. Molecular imaging of VEGF receptors in angiogenic vasculature with single-chain VEGF-based probes. Nature medicine. 2007; 13:504–509.

139. Rychak JJ, Graba J, Cheung AM, et al. Microultrasound molecular imaging of vascular endothelial growth factor receptor 2 in a mouse model of tumor angiogenesis. Molecular imaging. 2007; 6:289–296. [PubMed: 18092513]

140. Anderson CR, Rychak JJ, Backer M, et al. scVEGF microbubble ultrasound contrast agents: a novel probe for ultrasound molecular imaging of tumor angiogenesis. Investigative radiology. 2010; 45:579–585. [PubMed: 20733505]

141. Pochon S, Tardy I, Bussat P, et al. BR55: a lipopeptide-based VEGFR2-targeted ultrasound contrast agent for molecular imaging of angiogenesis. Investigative radiology. 2010; 45:89–95. [PubMed: 20027118]

142. Wijkstra H, Smeenge M, Rosette Jdl, et al. Targeted microbubble prostate cancer imaging with BR55. The 17th European Symposium on Ultrasound Contrast Imaging, Rotterdam. 2012:7–8.

143. Fry WJ, Mosberg WH Jr, Barnard JW, et al. Production of focal destructive lesions in the central nervous system with ultrasound. Journal of neurosurgery. 1954; 11:471–478. [PubMed: 13201985]

144. Hynynen K, Freund WR, Cline HE, et al. A clinical, noninvasive, MR imaging-monitored ultrasound surgery method. Radiographics : a review publication of the Radiological Society of North America, Inc. 1996; 16:185–195.

145. Medel R, Monteith SJ, Elias WJ, et al. Magnetic resonance-guided focused ultrasound surgery: Part 2: A review of current and future applications. Neurosurgery. 2012; 71:755–763. [PubMed: 22791029]

146. Ellens NP, Lucht BB, Gunaseelan ST, et al. A novel, flat, electronically-steered phased array transducer for tissue ablation: preliminary results. Phys Med Biol. 2015; 60:2195–2215. [PubMed: 25683789]

147. Tempany CM, Stewart EA, McDannold N, et al. MR imaging-guided focused ultrasound surgery of uterine leiomyomas: a feasibility study. Radiology. 2003; 226:897–905. [PubMed: 12616023]

148. Hurwitz MD, Ghanouni P, Kanaev SV, et al. Magnetic resonance-guided focused ultrasound for patients with painful bone metastases: phase III trial results. Journal of the National Cancer Institute. 2014; 106 dju082 1–9.

149. Xu Z, Carlson C, Snell J, et al. Intracranial inertial cavitation threshold and thermal ablation lesion creation using MRI-guided 220-kHz focused ultrasound surgery: preclinical investigation. Journal of neurosurgery. 2015; 122:152–161. [PubMed: 25380106]

150. Elias WJ, Huss D, Voss T, et al. A pilot study of focused ultrasound thalamotomy for essential tremor. The New England journal of medicine. 2013; 369:640–648. [PubMed: 23944301]

151. Lesser TG, Schubert H, Bischoff S, et al. Lung flooding enables efficient lung sonography and tumour imaging in human ex vivo and porcine in vivo lung cancer model. European journal of medical research. 2013; 18:23. [PubMed: 23841910]

152. Zhu H, Zhou K, Zhang L, et al. High intensity focused ultrasound (HIFU) therapy for local treatment of hepatocellular carcinoma: role of partial rib resection. European journal of radiology. 2009; 72:160–166. [PubMed: 18707834]

153. Bobkova S, Gavrilov L, Khokhlova V, et al. Focusing of high-intensity ultrasound through the rib cage using a therapeutic random phased array. Ultrasound Med Biol. 2010; 36:888–906. [PubMed: 20510186]

154. Simon JC, Sapozhnikov OA, Khokhlova VA, et al. Ultrasonic atomization of tissue and its role in tissue fractionation by high intensity focused ultrasound. Phys Med Biol. 2012; 57:8061–8078. [PubMed: 23159812]

155. Kieran K, Hall TL, Parsons JE, et al. Refining histotripsy: defining the parameter space for the creation of nonthermal lesions with high intensity, pulsed focused ultrasound of the in vitro kidney. The Journal of urology. 2007; 178:672–676. [PubMed: 17574617]

156. Tachibana K, Tachibana S. Albumin microbubble echo-contrast material as an enhancer for ultrasound accelerated thrombolysis. Circulation. 1995; 92:1148–1150. [PubMed: 7648659]

157. Sakharov DV, Barrertt-Bergshoeff M, Hekkenberg RT, et al. Fibrin-specificity of a plasminogen activator affects the efficiency of fibrinolysis and responsiveness to ultrasound: comparison of nine plasminogen activators in vitro. Thrombosis and haemostasis. 1999; 81:605–612. [PubMed: 10235448]

158. Aguiar MO, Tsutsui JM, Tavares BG, et al. Safety and feasibility of diagnostic ultrasound high mechanical index impulses in restoring epicardial flow in acute ST segment elevation myocardial infarction in humans. Proceedings of the 20th European Symposium on Ultrasound Contrast Imaging, Rotterdam. 2015; 20:185–186.

159. Barlinn K, Tsivgoulis G, Barreto AD, et al. Outcomes following sonothrombolysis in severe acute ischemic stroke: subgroup analysis of the CLOTBUST trial. International journal of stroke : official journal of the International Stroke Society. 2014; 9:1006–1010. [PubMed: 25079049]

160. Tachibana K, Tachibana S. Prototype therapeutic ultrasound emitting catheter for accelerating thrombolysis. Journal of ultrasound in medicine. 1997; 16:529–535. [PubMed: 9315208]

161. Unger EC, McCreery T, Sweitzer R, et al. MRX 501: a novel ultrasound contrast agent with therapeutic properties. Academic radiology. 1998; 5(Suppl 1):S247–S249. [PubMed: 9561092]

162. Tartis MS, McCallan J, Lum AF, et al. Therapeutic effects of paclitaxel-containing ultrasound contrast agents. Ultrasound Med Biol. 2006; 32:1771–1780. [PubMed: 17112963]

163. Rapoport NY, Kennedy AM, Shea JE, et al. Controlled and targeted tumor chemotherapy by ultrasound-activated nanoemulsions/microbubbles. Journal of controlled release : official journal of the Controlled Release Society. 2009; 138:268–276. [PubMed: 19477208]

164. Anwer K, Kao G, Proctor B, et al. Ultrasound enhancement of cationic lipid-mediated gene transfer to primary tumors following systemic administration. Gene therapy. 2000; 7:1833–1839. [PubMed: 11110415]

165. Klibanov AL, Shevchenko TI, Raju BI, et al. Ultrasound-triggered release of materials entrapped in microbubble-liposome constructs: a tool for targeted drug delivery. Journal of controlled release : official journal of the Controlled Release Society. 2010; 148:13–17. [PubMed: 20691227]

166. Escoffre JM, Mannaris C, Geers B, et al. Doxorubicin liposome-loaded microbubbles for contrast imaging and ultrasound-triggered drug delivery. IEEE transactions on ultrasonics, ferroelectrics, and frequency control. 2013; 60:78–87.

167. Yan F, Li L, Deng Z, et al. Paclitaxel-liposome-microbubble complexes as ultrasound-triggered therapeutic drug delivery carriers. Journal of controlled release : official journal of the Controlled Release Society. 2013; 166:246–255. [PubMed: 23306023]

168. Hynynen K, McDannold N, Vykhodtseva N, et al. Focal disruption of the blood-brain barrier due to 260-kHz ultrasound bursts: a method for molecular imaging and targeted drug delivery. Journal of neurosurgery. 2006; 105:445–454. [PubMed: 16961141]

169. Park J, Zhang Y, Vykhodtseva N, et al. The kinetics of blood brain barrier permeability and targeted doxorubicin delivery into brain induced by focused ultrasound. Journal of controlled release. 2012; 162:134–142. [PubMed: 22709590]

170. Nance E, Timbie K, Miller GW, et al. Non-invasive delivery of stealth, brain-penetrating nanoparticles across the blood-brain barrier using MRI-guided focused ultrasound. Journal of controlled release. 2014; 189:123–132. [PubMed: 24979210]

171. Jordao JF, Ayala-Grosso CA, Markham K, et al. Antibodies targeted to the brain with image-guided focused ultrasound reduces amyloid-beta plaque load in the TgCRND8 mouse model of Alzheimer's disease. PloS one. 2010; 5:e10549. [PubMed: 20485502]

172. Samiotaki G, Acosta C, Wang S, et al. Enhanced delivery and bioactivity of the neurturin neurotrophic factor through focused ultrasound-mediated blood-brain barrier opening in vivo. Journal of cerebral blood flow and metabolism. 2015; 35:611–622. [PubMed: 25586140]

173. Howles GP, Bing KF, Qi Y, et al. Contrast-enhanced in vivo magnetic resonance microscopy of the mouse brain enabled by noninvasive opening of the blood-brain barrier with ultrasound. Magnetic resonance in medicine. 2010; 64:995–1004. [PubMed: 20740666]

174. Aryal M, Vykhodtseva N, Zhang YZ, et al. Multiple treatments with liposomal doxorubicin and ultrasound-induced disruption of blood-tumor and blood-brain barriers improve outcomes in a rat glioma model. Journal of controlled release. 2013; 169:103–111. [PubMed: 23603615]

175. Leinenga G, Gotz J. Scanning ultrasound removes amyloid-beta and restores memory in an Alzheimer's disease mouse model. Science translational medicine. 2015; 7 278ra33.

176. Burgess A, Nhan T, Moffatt C, et al. Analysis of focused ultrasound-induced blood-brain barrier permeability in a mouse model of Alzheimer's disease using two-photon microscopy. Journal of controlled release. 2014; 192:243–248. [PubMed: 25107692]

177. Muller OJ, Schinkel S, Kleinschmidt JA, et al. Augmentation of AAV-mediated cardiac gene transfer after systemic administration in adult rats. Gene therapy. 2008; 15:1558–1565. [PubMed: 18615116]

178. Kotopoulis S, Delalande A, Popa M, et al. Sonoporation-enhanced chemotherapy significantly reduces primary tumour burden in an orthotopic pancreatic cancer xenograft. Molecular imaging and biology. 2014; 16:53–62. [PubMed: 23877869]

179. Kotopoulis S, Dimcevski G, Gilja OH, et al. Treatment of human pancreatic cancer using combined ultrasound, microbubbles, and gemcitabine: a clinical case study. Med Phys. 2013; 40:072902. [PubMed: 23822453]

180. Kotopoulis S, Dimcevski G, Hoem D, et al. Therapeutic ultrasound in pancreatic adenocarcinoma. The 20th European Symposium on Ultrasound Contrast Imaging, Rotterdam. 2015:28–29.

181. Chappell JC, Song J, Klibanov AL, et al. Ultrasonic microbubble destruction stimulates therapeutic arteriogenesis via the CD18-dependent recruitment of bone marrow-derived cells. Arteriosclerosis, thrombosis, and vascular biology. 2008; 28:1117–1122.

182. Wood AK, Bunte RM, Cohen JD, et al. The antivascular action of physiotherapy ultrasound on a murine tumor: role of a microbubble contrast agent. Ultrasound Med Biol. 2007; 33:1901–1910. [PubMed: 17720299]

183. Chin CT, Raju BI, Shevchenko T, et al. Control and reversal of tumor growth by ultrasound activated microbubbles. IEEE International Ultrasonics Symposium, Rome. 2009:77–80.

184. Todorova M, Agache V, Mortazavi O, et al. Antitumor effects of combining metronomic chemotherapy with the antivascular action of ultrasound stimulated microbubbles. International journal of cancer. 2013; 132:2956–2966.

185. Burks SR, Ziadloo A, Kim SJ, et al. Noninvasive pulsed focused ultrasound allows spatiotemporal control of targeted homing for multiple stem cell types in murine skeletal muscle and the magnitude of cell homing can be increased through repeated applications. Stem Cells. 2013; 31:2551–2560. [PubMed: 23922277]

186. Hannemann PF, Mommers EH, Schots JP, et al. The effects of low-intensity pulsed ultrasound and pulsed electromagnetic fields bone growth stimulation in acute fractures: a systematic review and meta-analysis of randomized controlled trials. Archives of orthopaedic and trauma surgery. 2014; 134:1093–1106. [PubMed: 24895156]

187. Gigliotti JC, Huang L, Bajwa A, et al. Ultrasound Modulates the Splenic Neuroimmune Axis in Attenuating AKI. Journal of the American Society of Nephrology. 2015 JASN.2014080769.

188. Gigliotti JC, Huang L, Ye H, et al. Ultrasound prevents renal ischemia-reperfusion injury by stimulating the splenic cholinergic anti-inflammatory pathway. Journal of the American Society of Nephrology : JASN. 2013; 24:1451–1460. [PubMed: 23907510]

189. Legon W, Sato TF, Opitz A, et al. Transcranial focused ultrasound modulates the activity of primary somatosensory cortex in humans. Nature neuroscience. 2014; 17:322–329. [PubMed: 24413698]

Figure 1.
Portable ultrasound equipment. (Left) “SonicWindow” Handheld C-scan device (Reprinted with permission, image courtesy of Analogic, Copyright, 2014) (Right) “V-Scan” Handheld B-scan device (Reprinted with permission, image courtesy of GE Healthcare, Copyright 2013)

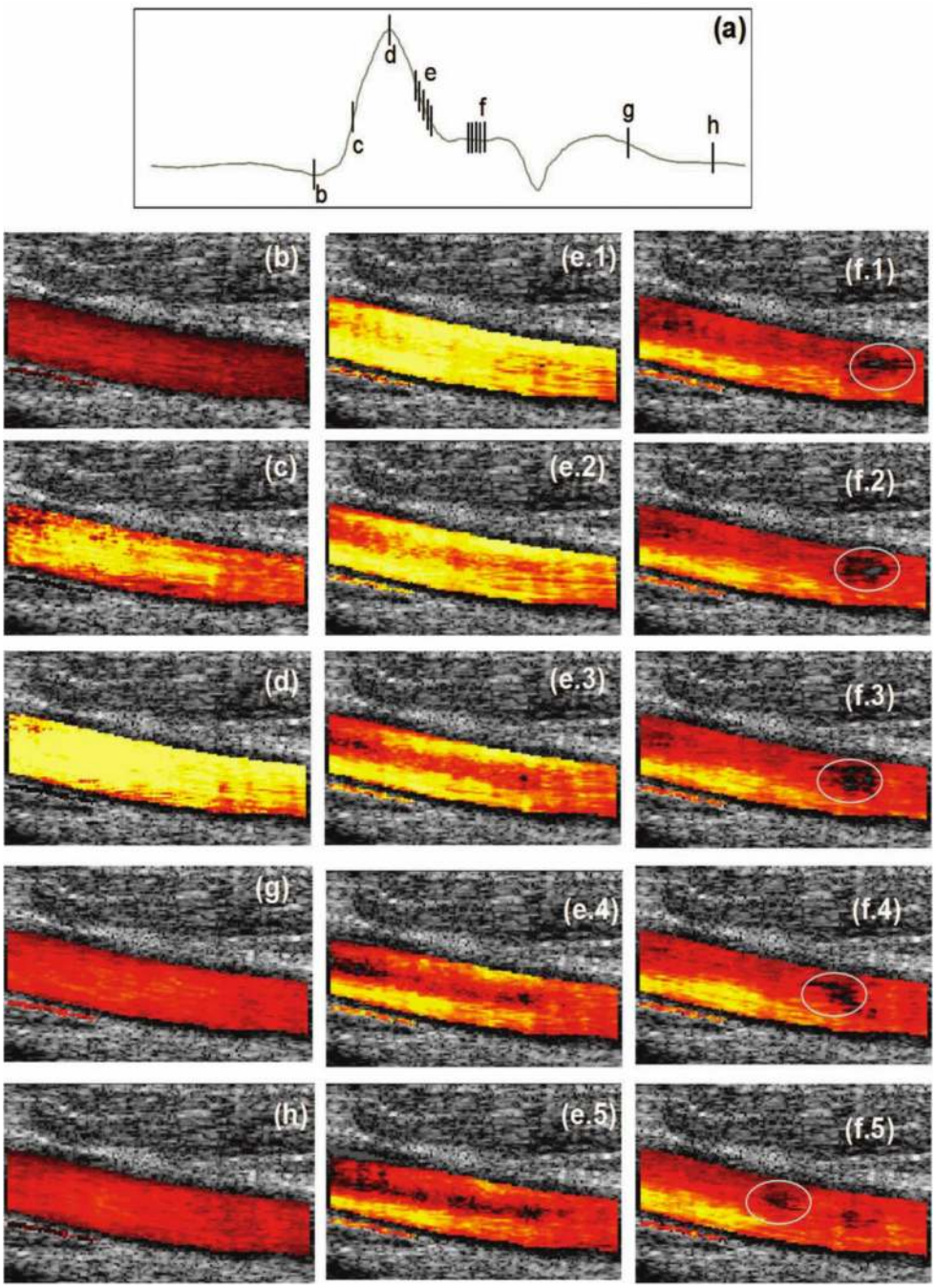

Figure 2.
Selected frames from a cardiac cycle obtained with using ultrafast compound Doppler. (a) Average flow in the artery indicating the selected frames. (b) Before the opening of the aortic valve, there is a minimal laminar flow. (c) and (d) Acceleration of the flow. (e) Inversion of the parabolic profile in the deceleration. (f) Local turbulence is present and propagates in the artery. (g) and (h) Laminar flows in diastole. Reprinted with permission from [61], Copyright, 2011, IEEE.

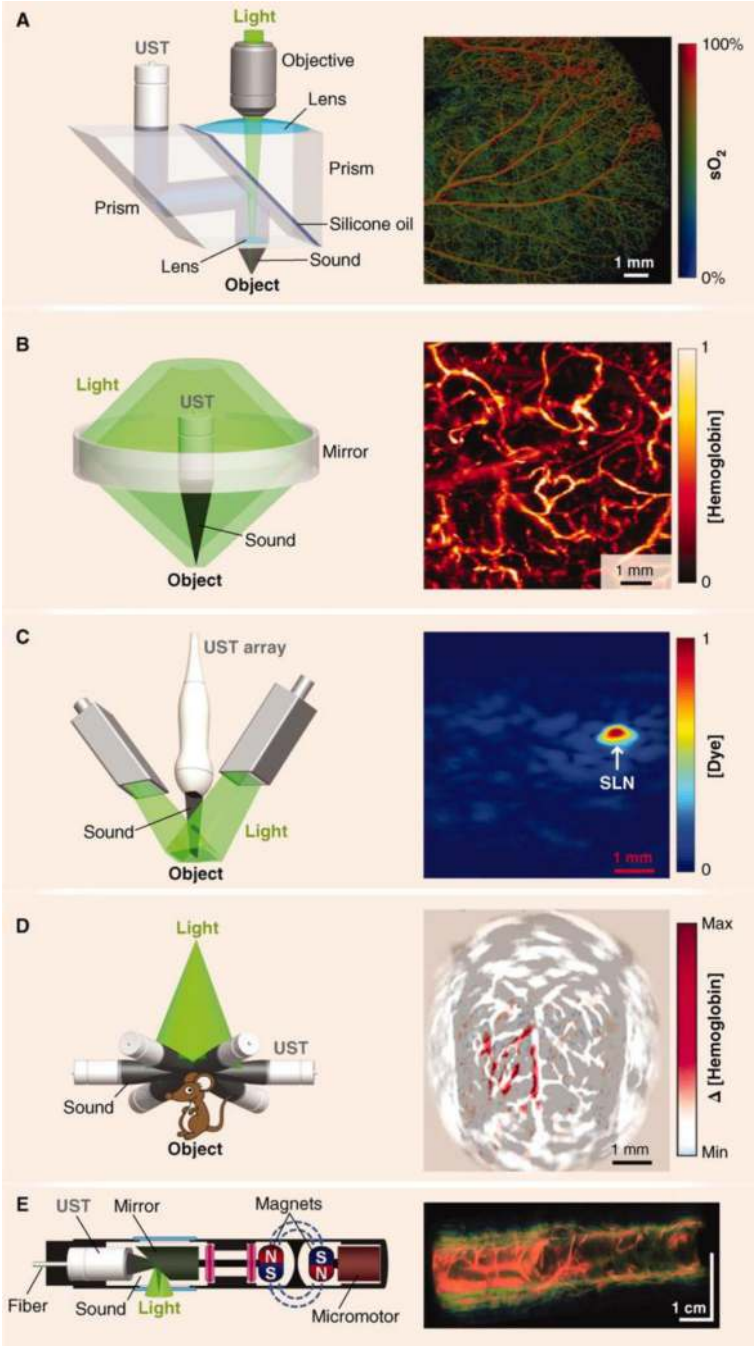

Figure 3.

Components of Photoacoustic Tomography, with representative in vivo images across multiple resolution scales (A) Optical Resolution Photoacoustic Microscopy of sO2 in a mouse ear. (B) Acoustic Resolution Photoacoustic Microscopy of normalized total hemoglobin concentration, [hemoglobin], in a human palm. (C) Linear-array Photoacoustic Computed Tomography of normalized Methylene Blue concentration, [dye], in a rat sentinel lymph node (SLN). (D) Circular-array Photoacoustic Computed Tomography of cerebral hemodynamic changes, Δ [hemoglobin], in response to one-sided whisker stimulation in a

rat. (E) Photoacoustic endoscopy of a rabbit esophagus and adjacent internal organs, including the trachea and lung. UST, ultrasonic transducer. Reprinted with permission from [100]; Copyright, 1012, American Association for the Advancement of Science.

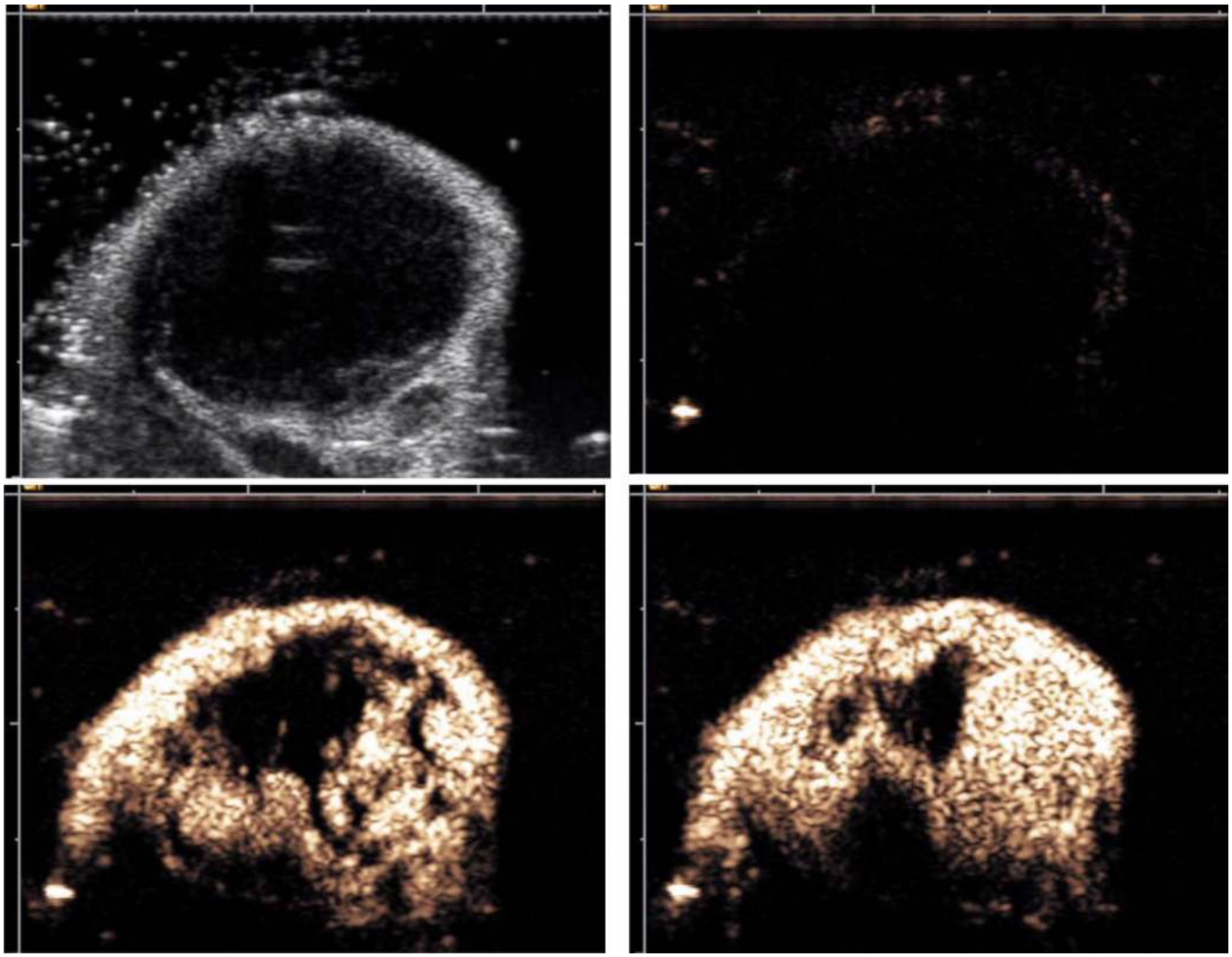

Figure 4.

Ultrasound imaging of subcutaneneous tumor in a murine model. Top Left: B-mode grayscale imaging (anatomy). Top Right: contrast mode (Cadence CPS), prior to microbubble administration. Bottom Left: contrast mode (Cadence CPS), following microbubble administration (at peak, ∼5 sec following iv bolus). Bottom Right: contrast mode (Cadence CPS), following microbubble administration (at peak, ∼30 sec following iv bolus). Imaging performed with Sequoia 512 scanner equipped with 15L8 probe.

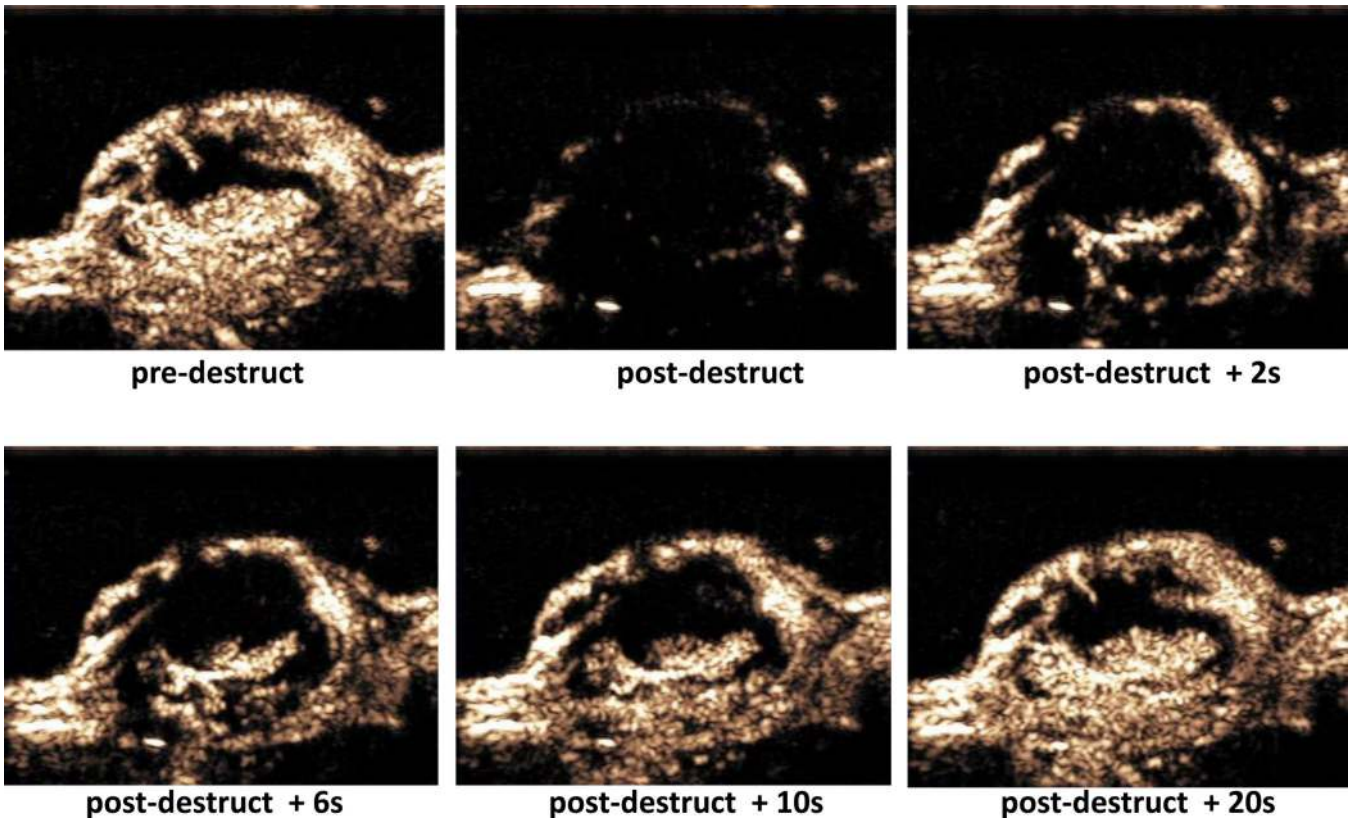

Figure 5.

Contrast ultrasound imaging of tumor vasculature perfusion in destruction-replenishment mode in a subcutaneous murine tumor model. Top Left: microbubbles within the tumor vasculature after intravenous administration, prior to the destructive pulse. Top Center: immediately after 2 s destructive pulse. Top Right: 2 s after cessation of the destructive pulse. Bottom Right: 6 s after destructive pulse. Bottom Center: 10 s after destructive pulse. Bottom Right: 20 s after destructive pulse. Imaging performed with Sequoia 512 scanner equipped with 15L8 probe (7 MHz, MI 0.2 for imaging, MI 1.9 for destruction).

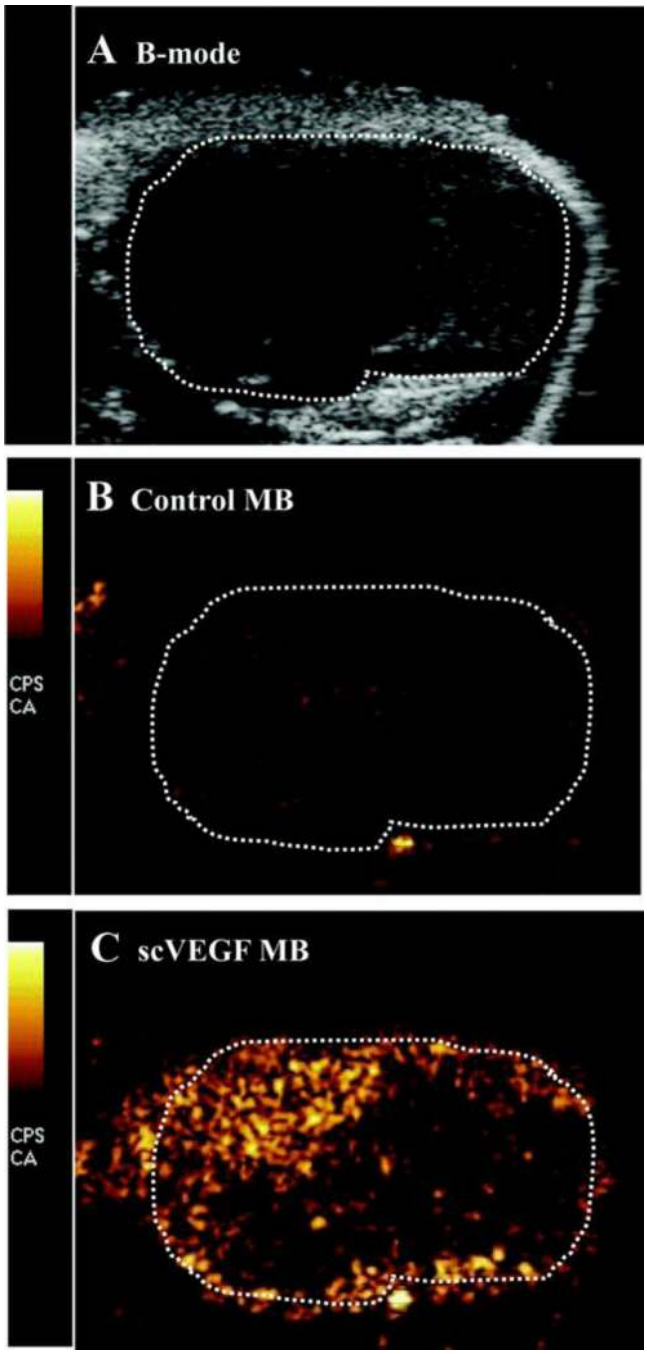

Figure 6.

Ultrasound Molecular Imaging of VEGFR2 with scVEGF-decorated microbubbles. Ultrasound imaging of subcutaneous colon adenocarcinoma. A, B-mode US image of tumor tissue marked by dotted line. B, Contrast US image of nontargeted MB after 6-minute dwell time. C, Contrast US image illustrates higher pixel intensity because of adherent scVEGF-MB. Copyright, 2010, Lippincott, Williams and Wilkins, reprinted with permission from reference [140].

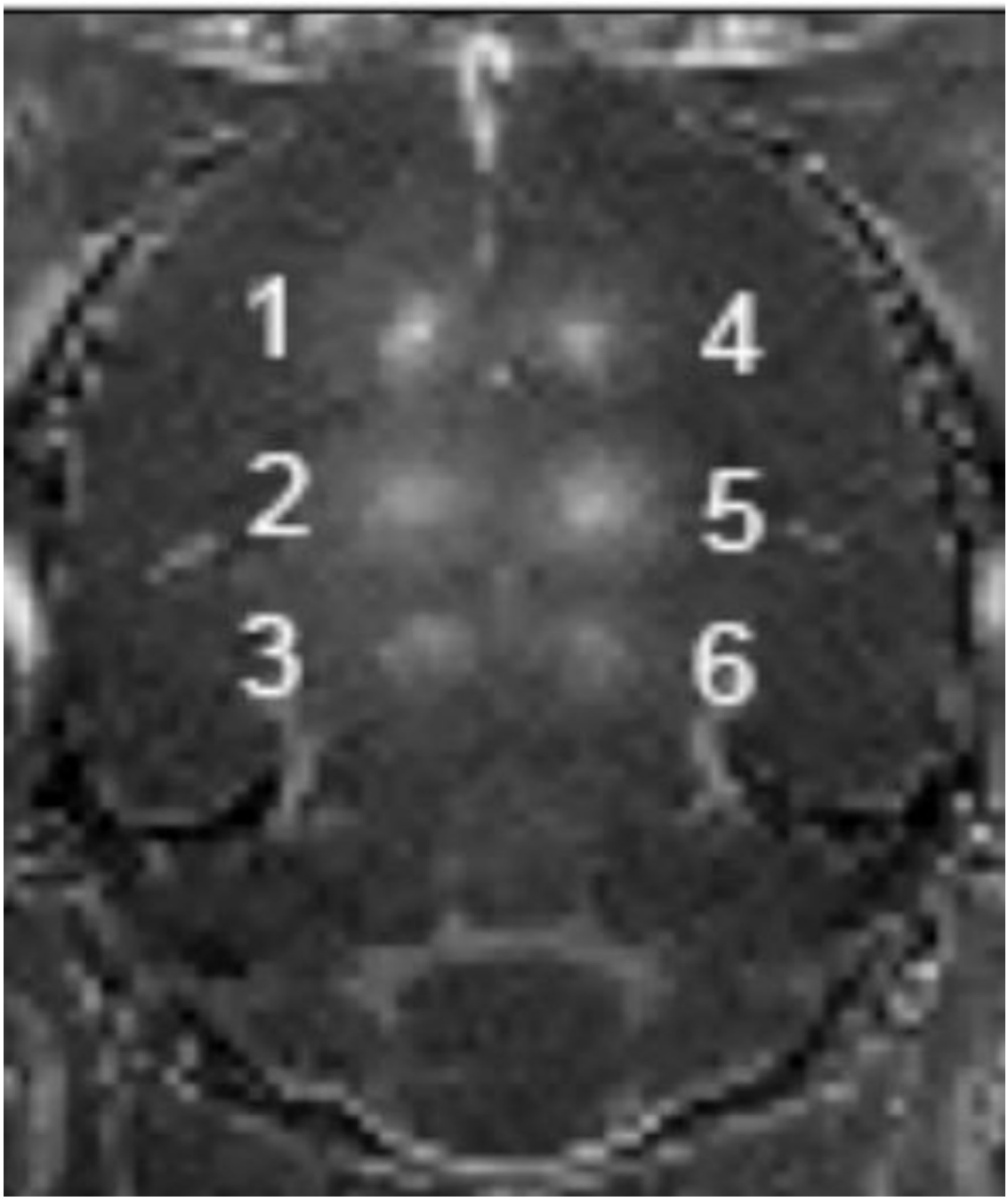

Figure 7.

Ultrasound-induced opening of blood brain barrier in a rat model. Decafluorobutane microbubbles (stabilized with DSPC and PEG Stearate) were injected intravenously, immediately followed by focused ultrasound treatment (IGT, 1 Hz, 20ms pulses, 1–2 min treatment duration) and intravenous administration of Gd-DTPA. MRI contrast extravasation and accumulation (white focal spots in the center of the image) observed minutes after ultrasound treatment and Gd-DTPA administration. Imaging performed at

UVA Molecular Imaging Center (7T MRI Clinscan, Bruker/Siemens). Copyright, Max Wintermark, 2014, reprinted with permission.